Journal of Medicinal Chemistry

Article

Design, synthesis and evaluation of reversible and irreversible monoacylglycerol lipase positron emission tomography (PET) tracers using a 'tail switching' strategy on a piperazinyl azetidine skeleton

Zhen Chen, Wakana Mori, XIAOYUN DENG, Ran Cheng, Daisuke Ogasawara, Genwei Zhang, Michael Andreas Schafroth, Kenneth Dahl, Hualong Fu, Akiko Hatori, Tuo Shao, Yiding Zhang, Tomoteru Yamasaki, Xiaofei Zhang, Jian Rong, Qingzhen Yu, Kuan Hu, Masayuki Fujinaga, Lin Xie, Katsushi Kumata, Yuancheng Gou, Jingjin Chen, Shuyin Gu, Liang Bao, Lu Wang, Thomas Lee Collier, Neil Vasdev, Yihan Shao, Jun-An Ma, Benjamin F. Cravatt, Christopher Fowler, Lee Josephson, Ming-Rong Zhang, and Steven H Liang

J. Med. Chem., **Just Accepted Manuscript** • DOI: 10.1021/acs.jmedchem.8b01778 • Publication Date (Web): 04 Mar 2019

Just Accepted

ACS Publications

is published by the American Chemical Society. 1155 Sixteenth Street N.W., Washington, DC 20036

	Fujinaga, Masayuki; Department of Radiopharmaceuticals Development, National Institute of Radiological Sciences, National Institutes for Quantum and Radiological Science and Technology Xie, Lin; Kokuritsu Kenkyu Kaihatsu Hojin Hoshasen Igaku Sogo Kenkyujo, Radiopharmaceuticals Development Kumata, Katsushi; Kokuritsu Kenkyu Kaihatsu Hojin Hoshasen Igaku Sogo Kenkyujo, Department of Radiopharmaceuticals Development Gou, Yuancheng; ChemShuttle, Inc. Chen, Jingjin; ChemShuttle, Inc. Gu, Shuyin; ChemShuttle, Inc. Bao, Liang; ChemShuttle, Inc. Wang, Lu; Division of Nuclear Medicine and Molecular Imaging, Massachusetts General Hospital & Department of Radiology, Harvard Medical School Collier, Thomas; Division of Nuclear Medicine and Molecular Imaging, Massachusetts General Hospital & Department of Radiology, Harvard Medical School Vasdev, Neil; Harvard Medical School/Massachusetts General Hospital, Nuclear Medicine and Molecular Imaging Shao, Yihan; University of Oklahoma, Chemistry & Biochemistry Ma, Jun-An; Tianjin University, Department of Chemistry Cravatt, Benjamin; Scripps Research Institute, Chemical Physiology; The Scripps Research Institute, Department of Chemical Physiology Fowler, Christopher; Department of Pharmacology and Clinical Neuroscience, Umeå University Josephson, Lee; Division of Nuclear Medicine and Molecular Imaging, Massachusetts General Hospital & Department of Radiology, Harvard Medical School Zhang, Ming-Rong; National Institute of Radiological Sciences, Department of Radiopharmaceuticals Development Liang, Steven; Mass General Hospital and Harvard Medical School,

Design, synthesis and evaluation of reversible and irreversible monoacylglycerol lipase positron emission tomography (PET) tracers using a 'tail switching' strategy on a piperazinyl azetidine skeleton

Zhen Chen,[1,2,#] Wakana Mori,[3,#] Xiaoyun Deng,[1] Ran Cheng,[1] Daisuke Ogasawara,[4] Genwei Zhang,[5] Michael A. Schafroth,[4] Kenneth Dahl,[1] Hualong Fu,[1] Akiko Hatori,[3] Tuo Shao,[1] Yiding Zhang,[3] Tomoteru Yamasaki,[3] Xiaofei Zhang,[1] Jian Rong,[1] Qingzhen Yu,[1] Kuan Hu,[3] Masayuki Fujinaga,[3] Lin Xie,[3] Katsushi Kumata,[3] Yuancheng Gou,[6] Jingjin Chen,[6] Shuyin Gu,[6] Liang Bao,[6] Lu Wang,[1] Thomas Lee Collier,[1] Neil Vasdev,[1] Yihan Shao,[5] Jun-An Ma,[2] Benjamin F. Cravatt,[4] Christopher Fowler,[7] Lee Josephson,[1] Ming-Rong Zhang[3,*] and Steven H. Liang[1,*]

[1]Division of Nuclear Medicine and Molecular Imaging, Massachusetts General Hospital & Department of Radiology, Harvard Medical School, Boston, MA, 02114, USA.

[2]Department of Chemistry, School of Science, Tianjin University, 92 Weijin Road, Nankai District, Tianjin 300072, China

[3]Department of Radiopharmaceuticals Development, National Institute of Radiological Sciences, National Institutes for Quantum and Radiological Science and Technology, Chiba, 263-8555, Japan.

[4]The Skaggs Institute for Chemical Biology and Department of Chemical Physiology, The Scripps Research Institute, SR107 10550 North Torrey Pines Road, La Jolla, California 92037, USA

[5]Department of Chemistry and Biochemistry, University of Oklahoma, Norman, Oklahoma 73019, USA.

[6]ChemShuttle, Inc., 1699 Huishan Blvd., Wuxi, Jiangsu, 214174, China

[7]Department of Pharmacology and Clinical Neuroscience, Umeå University, SE-901 87 Umeå, Sweden

[#]These authors contribute equally to this work.

Abstract: Monoacylglycerol lipase (MAGL) is a serine hydrolase that degrades 2-arachidonoylglycerol (2-AG) in the endocannabinoid system (eCB). Selective inhibition of MAGL has emerged as a potential therapeutic approach for the treatment of diverse pathological conditions including chronic pain, inflammation, cancer and neurodegeneration. Herein we disclose a novel array of reversible and irreversible MAGL inhibitors by means of tail switching on a piperazinyl azetidine scaffold. We developed a lead irreversible-binding MAGL inhibitor **8**, and reversible-binding compounds **17** and **37** which are amenable for radiolabeling with ^{11}C or ^{18}F. [^{11}C]**8** ([^{11}C]MAGL-2-11) exhibited high brain uptake and excellent binding specificity in the brain towards MAGL. Reversible radioligands [^{11}C]**17** ([^{11}C]PAD) and [^{18}F]**37** ([^{18}F]MAGL-4-11) also demonstrated excellent *in vivo* binding specificity towards MAGL in peripheral organs. This work may pave the way for the development of MAGL-targeted positron emission tomography (PET) tracers with tunability in reversible and irreversible binding mechanism.

Keywords: monoacylglycerol lipase; MAGL; 2-AG; positron emission tomography; irreversible; reversible;

INTRODUCTION

As a lipid signaling network, membrane-bound G-coupled cannabinoid receptors, namely CB_1 and CB_2, and their endogenous ligands, 2-arachidonoylglycerol (2-AG) and *N*-arachidonoylethanolamine (AEA) established the backbone of endocannabinoid (eCB) system.[1-5] The eCB system is prominent in both the central and peripheral nervous system, and its dysfunction has been implicated in a wide range

of pathological conditions including pain, appetite, inflammation, memory and cognition, and cancer.[6-10] Since direct regulation of CB_1 receptors is often accompanied with a series of debilitating adverse effects such as substance abuse, loss of motor and cognition functions,[11, 12] recent drug discovery efforts have been shifted to regulating the levels of AEA or 2-AG. As the most essential endogenous ligands with endocannabinoid-like activity, AEA and 2-AG are synthesized "on request" *in vivo* and in the brain primarily degraded by fatty acid amide hydrolase (FAAH) and monoacylglycerol lipase (MAGL), respectively.[13-16] In particular, MAGL belongs to serine hydrolase superfamily, which is associated with the eCB system as well as eicosanoid and other lipid signaling pathways.[17] In rodents, MAGL is highly expressed in the CNS as well as several peripheral organs including liver, kidney, adrenal glands and brown adipose tissue.[18] In humans, there is a similar CNS MAGL distribution to that in rodents with high levels of activity in the cerebral cortex, hippocampus and cerebellum, and low levels in the hypothalamus and pons.[19] Considering its prime role in 2-AG hydrolysis in the brain, selective inhibition of MAGL may represent an alternative and potential therapeutic target for treatment of diverse pathological conditions including chronic pain, inflammation, cancer and neurodegeneration without apparent side effects related with direct CB_1 regulation.[20-31]

Positron emission tomography (PET) is a non-invasive and highly sensitive technology in the realm of molecular imaging, and serves as an ideal tool to quantify biochemical and pharmacological processes *in vivo* under normal and disease conditions.[32-34] PET studies of MAGL would allow to achieve in-depth knowledge of MAGL-related pathological changes between normal and disease state, and in vivo interaction of novel MAGL inhibitors with the target. Development of MAGL PET tracers would remarkably help to validate promising MAGL inhibitors in clinical trials. As a result, in the past few years, considerable efforts have been exerted towards this goal despite still with limited success.

The first attempt for PET imaging of MAGL was performed by Hicks *et al.* with several carbon-11 labeled MAGL inhibitors, including [^{11}C]KML29, and [^{11}C]JJKK-0048. However, all these compounds had limited brain uptake, which impeded their further translation.[35] To date, only three potent MAGL PET tracers,[36] namely [^{11}C]SAR127303,[37-39] [^{11}C]MA-PB-1[40] based on a piperidyl carbamate scaffold, and [^{11}C]MAGL-0519[41] based on an azetidinyl oxadiazole scaffold, have been developed to image MAGL in living brains of rats and non-human primates (NHPs) (**Figure 1A**). However, most reported MAGL PET tracers are highly lipophilic (cLogP ca. 3-5), which is often linked with fast metabolic clearance, poor *in vivo* stability, and high propensity for off-target promiscuity.[42, 43] For example, the 2,5-regioisomer of LY2183240 exhibited poor selectivity between MAGL and FAAH, which could be, in some extent, attributed to a high cLogP value of 4.03.[43] Furthermore, the binding mechanism of these PET tracers was limited to be irreversible and no reversible MAGL PET ligand has been reported to date. In fact, a reversible MAGL tracer would enable the access to critical quantitative kinetic analysis, including facilitated measures of binding potential and volume of distribution, for monitoring neurological response to therapeutics.[44, 45] As a result, there is a critical demand for the development of both irreversible and reversible MAGL PET tracers with favorable lipophilicity and brain kinetics.

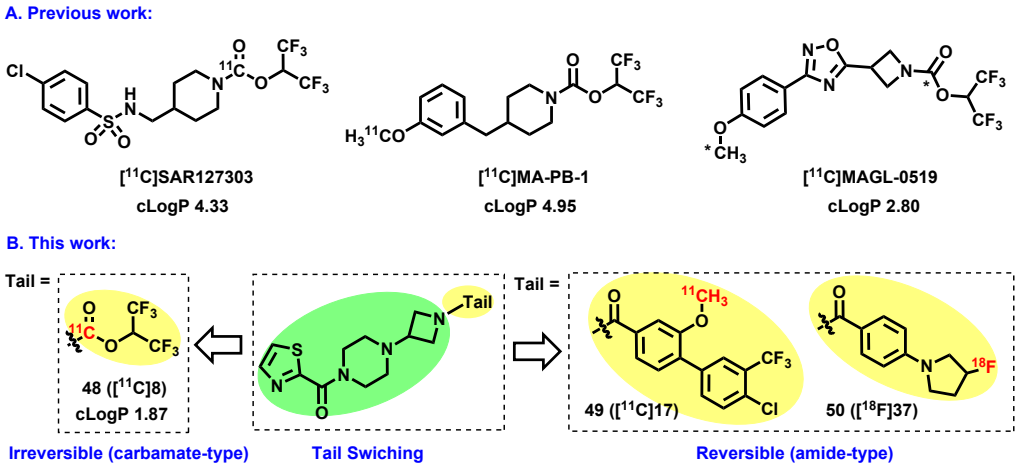

Figure 1. Representative PET tracers for imaging brain MAGL and our work.

As part of our continuing interest in the development and translation of novel MAGL PET tracers,[37, 39, 41] herein we described a novel class of MAGL inhibitors using a 'tail switching' strategy,[46, 47] wherein the 'tail' refers to the group that is attached to the unique piperazinyl azetidine skeleton (**Figure 1B**).[48-50] In detail, our medicinal efforts focused on the synthesis of an array of (4-(azetidin-3-yl)piperazin-1-yl)(thiazol-2-yl)methanone derived carbamates or ureas as irreversible candidate MAGL inhibitors and (4-(azetidin-3-yl)piperazin-1-yl)(thiazol-2-yl)methanone derived amides as reversible candidates, with amenability for radiolabeling with carbon-11 or fluorine-18. Pharmacological studies, molecule docking and physicochemical evaluations were performed to identify our compound **8** as the most promising irreversible MAGL inhibitor, and compounds **17** & **37** as the most promising reversible MAGL inhibitors, worthy of radiolabeling and *in vivo* PET translational studies. With innovative and efficient ^{11}C- and ^{18}F-labeling strategies, we evaluated the brain permeability, binding specificity and kinetics of these lead radioligands **48** ([^{11}C]**8**), **49** ([^{11}C]**17**) and **50** ([^{11}C]**37**) by PET experiments in rodents. While irreversible MAGL tracer **48** demonstrated excellent in vitro potency and selectivity, in vivo binding specificity and stability in the brain, our reversible MAGL tracers **49** and **50** demonstrated high-level specific binding to MAGL in a peripherally-restricted manner. As proof-of-concept, we were able to unveil the underlying cause of low brain accumulation for **49** and **50**, the most potent reversible MAGL tracers in our design, thus paving the way for future development of reversible MAGL PET tracers.

RESULTS AND DISCUSSION

Chemistry. A focused library of (4-(azetidin-3-yl)piperazin-1-yl)(thiazol-2-yl)methanone derived carbamates or ureas **8-13** as irreversible MAGL inhibitor candidates and (4-(azetidin-3-yl)piperazin-1-yl)(thiazol-2-yl)methanone derived amides **16-22**, **36-38** as reversible MAGL inhibitor candidates were synthesized, the scaffold of which are amenable for ^{11}C- or ^{18}F-labeling. As summarized in **Scheme 1**, the S_N2 displacement reaction between *tert*-butyloxycarbonyl (Boc)-protected piperazine **1** and 1-benzhydrylazetidin-3-yl methanesulfonate **2** readily proceeded to give **3** in 85% yield. Trifluoroacetic acid (TFA)-induced deprotection of the Boc group from **3** led to isolation of **4** in nearly quantitative yield, which subsequently coupled with thiazole-2-carboxylic acid **5** to produce **6** in high efficiency in the presence of 1-hydroxybenzotriazole hydrate (HOBT) and *N*-(3-dimethylaminopropyl)-*N*'-ethylcarbodiimide hydrochloride (EDC•HCl). 1-Chloroethyl chloroformate triggered deprotection of the diphenylmethyl group from **6** released azetidine **7** in 86% yield, which served as a crucial precursor for the following ^{11}C-labeling. To synthesize irreversible MAGL inhibitor candidates **8-13**, we deployed several parallel approaches for the introduction of different carbonyl-R groups. The combination of 1,1,1,3,3,3-hexafluoro-2-propanol, 4-nitrophenyl chloroformate, 4-dimethylaminopyridine (DMAP), pyridine and Et_3N in CH_2Cl_2 proved optimal to generate **8** in 20% yield. For candidates **9-12**, triphosgene was found to be a superior activating reagent, thus producing the corresponding carbamates **9** and **12**, as well as triazolyl carbonyls **10** and **11** in 7-43% yields. Candidate **13** was isolated in 13% yield by the treatment of azetidine **7** with *N*,*N*′-disuccinimidyl carbonate.

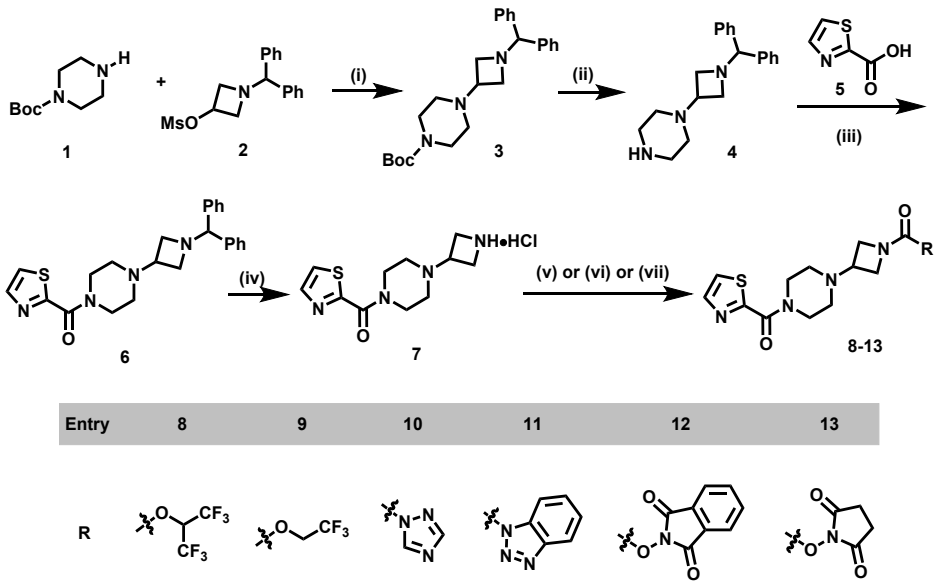

Scheme 1. Synthesis of irreversible MAGL inhibitors **8-13**. Conditions: (i) DIPEA, MeCN, 80 ^{o}C for 12 h; 85% yield; (ii) TFA, CH_2Cl_2, rt, 12 h; 99% yield; (iii) HOBT, EDC•HCl, Et_3N, DMF, rt, 12 h; 78% yield; (iv) 1-chloroethyl chloroformate, CH_2Cl_2, rt, 2 h; then MeOH, 35 ^{o}C 2 h; 86% yield; (v) 1,1,1,3,3,3-hexafluoro-2-propanol, 4-nitrophenyl chloroformate, DMAP, pyridine, Et_3N, CH_2Cl_2, rt, 5 h; 20% yield for **8**; (vi) 2,2,2-trifluoroethanol (for **9**) or 1,2,4-triazole (for **10**) or 1*H*-benzo[*d*][1,2,3]triazole (for **11**) or 2-hydroxyisoindoline-1,3-dione (for **12**), triphosgene, DMAP, Et_3N, CH_2Cl_2, rt, 4 h; 43% yield for **9**; 28% yield for **10**; 7% yield for **11**; 29% yield for **12**; (vii) *N*,*N*′-disuccinimidyl carbonate, Et_3N, CH_2Cl_2, rt, overnight; 14% yield for **13**; DIPEA = *N*,*N*-diisopropylethylamine; TFA = trifluoroacetic acid; HOBT = 1-hydroxybenzotriazole hydrate; EDC•HCl = *N*-(3-dimethylaminopropyl)-*N*′-ethylcarbodiimide hydrochloride; Et_3N = triethylamine; DMF = *N*,*N*-dimethylformamide; DMAP = 4-dimethylaminopyridine.

To synthesize reversible candidate MAGL inhibitors **16-22** and **36-38**, methyl 4-bromo-3-methoxybenzoate was used as the starting material (**Scheme 2A**). Cross-coupling reactions with aryl boronic acid followed by LiOH-mediated hydrolysis readily provided [1,1'-biaryl]-4-carboxylic acid **15** in 32-89% yield over two steps. For Suzuki-type reactions with phenyl boronic acids, $Pd(PPh_3)$ proved to be the optimal catalyst, while in the case of heteroaryl boronic acids as coupling partners, $PdCl_2$(dppf)

was utilized to provide good yields. Subsequent coupling reactions of **15** with piperazinyl azetidine **7** in the presence of HOBT and EDC•HCl proceeded smoothly to give amide-type MAGL inhibitors **16-22** in 21-40% yields. For the synthesis of **36-38**, ethyl 4-fluorobenzoate was utilized as the starting material (**Scheme 2B**). Amination reactions with hydroxyl azetidine, hydroxyl pyrazole or hydroxyl piperidine occurred smoothly under basic conditions, thus delivering **24-26** in moderate to high efficiencies (38-82% yields). Activation of the hydroxyl group by treatment with methane sulfonyl chloride afforded the mesylate compounds **27-29** in excellent yields (80-84%), which were readily fluorinated by tetrabutylammonium fluoride (TBAF) to generate **30-32** in 23-38% yields. The poor yields observed in the fluorination reactions can likely be attributed to the propensity of β-elimination of methanesulfonate derivatives **27-29** under basic conditions. Ultimately, candidates **36-38** were obtained in 18-28% yield over two steps, namely LiOH-promoted hydrolysis of **30-32** followed by condensation with piperazinyl azetidine **7**.

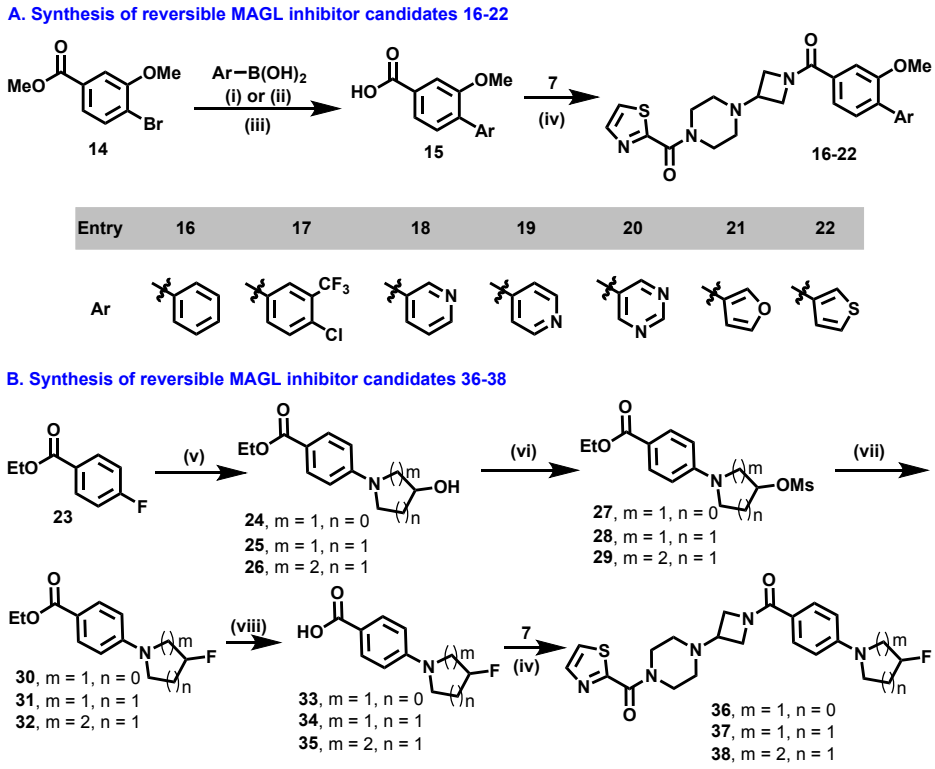

Scheme 2. Synthesis of reversible MAGL inhibitors **16-22** and **36-38**. Conditions: (i) $Pd(PPh_3)_4$, K_2CO_3, toluene/H_2O, 100 °C, overnight; (ii) $PdCl_2$(dppf), K_2CO_3, 1,4-dioxane/H_2O, 105 °C, overnight; (iii) LiOH, THF/H_2O, rt, overnight; (iv) HOBT, EDC•HCl, Et_3N, DMF, rt, 12 h; 22% yield for **16**; 25% yield for **17**; 21% yield for **18**; 23% yield for **19**; 24% yield for **20**; 39% yield for **21**; 40% yield for **22**; 32% yield for **36**; 30% yield for **37**; 19% yield for **38**; (v) azetidin-3-ol hydrochloride (for **24**) or pyrrolidin-3-ol hydrochloride (for **25**) or piperidin-4-ol (for **26**), K_2CO_3, DMSO, 180 °C for 2 h (for **24**) or 120 °C for 24 h (for **25** and **26**); 38% yield for **24**; 79% yield for **25**; 82% yield for **26**; (vi) MsCl, Et_3N, CH_2Cl_2, rt, overnight; 81% yield for **27**; 84% yield for **28**; 80% yield for **29**; (vii) TBAF, THF, 70 °C, 2 h; 23% yield for **30**; 38% yield for **31**; 26% yield for **32**; (viii) LiOH, THF/MeOH/H_2O, 40 °C, 16 h; 73% yield for **33**; 92% yield for **34**; 95% yield for **35**; dppf = 1,1′-bis(diphenylphosphino)ferrocene; HOBT = 1-hydroxybenzotriazole hydrate; EDC•HCl = *N*-(3-Dimethylaminopropyl)-*N*′-ethylcarbodiimide hydrochloride; DMF = *N*,*N*-dimethylformamide; DMSO = methyl sulfoxide; MsCl = methanesulfonyl chloride; TBAF = tetrabutylammonium fluoride.

Pharmacology. Compounds **8-13**, **16-22** and **36-38** were investigated for their potency and selectivity towards MAGL in vitro. For irreversible candidates **8-13**, we determined their in vitro ability to inhibit MAGL hydrolysis of [^{3}H]2-oleoylglycerol ([^{3}H]2-OG), a tritiated 2-AG analog, according to our previously reported protocol.[51] As outlined in **Table 1**, **Figure 2A** and **Figure S1**, candidate **8** containing a hexafluoroisopropanol leaving group demonstrated the most promising potency towards inhibition of MAGL activity with an IC_{50} value to be 0.88 nM, whereas all of the other candidates **9-13** indicated inferior potency (**Figure S1**). The residual activity seen in Figure 2B reflects the fact that whilst is the predominant hydrolytic enzyme in the brain, it is not the only one: Blankman et al.[15] reported that MAGL was responsible for ~85% of the hydrolysis of 2-AG in the brain, and the present data is consistent with this report. Inhibitor **8** exhibited preincubation-time-dependent inhibition at three tested concentrations (0.3, 1 and 3 nM, **Figure 2B**), which is in line with the irreversible binding mechanism. Although compound **10** possessing a triazole leaving group also exhibited good potency (IC_{50} =10 nM), no further evaluation was conducted considering the poor blood-brain barrier (BBB) penetration ability for an irreversible MAGL PET tracer with a triazole leaving group.[39]

Entry	8	9	10	11	12	13	MAGL-0519
IC_{50} (nM)	0.88 ± 0.05	> 1000	10.0 ± 4.2	87.1 ± 12.4	>1000	27.5 ± 8.1	8.4 ± 0.2

Table 1. IC_{50} values of compounds **8-13** for inhibition of MAGL activity with MAGL-0519, a known irreversible MAGL inhibitor, as reference.

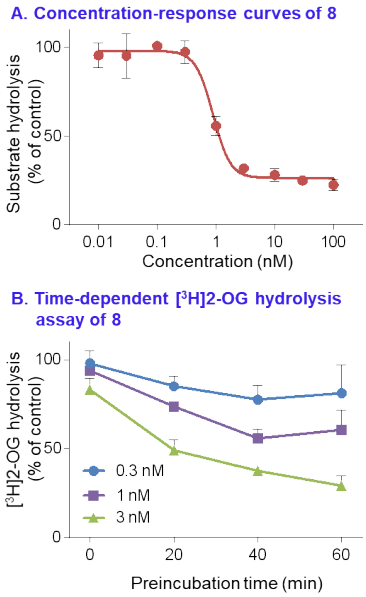

Figure 2. (A) Concentration-response curses of **8** for inhibition of [^{3}H]2-OG hydrolysis by rat brain MAGL (1 h preincubation between enzyme source and inhibitor prior to addition of substrate); (B) Time-dependent inhibition of [^{3}H]2-OG hydrolysis at three different concentrations (0.3, 1 and 3 nM).

For reversible candidates **16-22** and **36-38**, we initially evaluated their potency towards MAGL at a single concentration of 1 μM utilizing two different assays: (1) activity-based protein profiling (ABPP) studies and (2) hydrolysis of [^{3}H]2-OG. As depicted in **Figure 3A** and **S2**, both methods demonstrated compounds **17**, **37** and **38** as the most potent MAGL inhibitors. The IC_{50} values of candidates **17**, **37** and **38** were further determined as 2.7 nM, 11.7 nM and 15.0 nM, respectively, via ABPP assays (**Figure 3B**). As proof-of-concept, the reversibility of binding mechanism for candidates **17** and **37** was further investigated. In the case of **17**, we utilized an ABPP assay (**Figure 3C**). In this case, enzyme activity was measured by treatment with FP-rhodamine. For a reversible inhibitor, the compound would compete with FP-rhodamine, and each dissociation from the enzyme would present a new target for FP-rhodamine. Therefore, for reversible inhibitors, the levels of MAGL labeled with FP-rhodamine would increase over time. This was shown to be the case for **17**, but not for the irreversible inhibitor MJN110.

In the case of **37**, we investigated the mode of inhibition using [^{3}H]2-OG as substrate (**Figures 3D, E**). There was no preincubation time-dependent increase in observed inhibition of the 2-OG hydrolytic activity of the samples, which would have been expected for an irreversible inhibitor (**Figure 3D**). Jump dilution experiments, whereby samples are preincubated with inhibitor and then diluted prior to addition of substrate suggested no recovery of inhibition following a 20-fold dilution (**Figure 3E**). However, this behavior can be found under certain conditions (K_i^{app}/[E]≥10, short incubation times with substrate) for tight-binding reversible inhibitors when the high potency is due to longer residence times, i.e. slower rates of dissociation.[52] Based on these preliminary results, we selected **17** for ^{11}C-labeling, and **37** for ^{18}F-labeling, as lead reversible inhibitors for further in vivo evaluation.

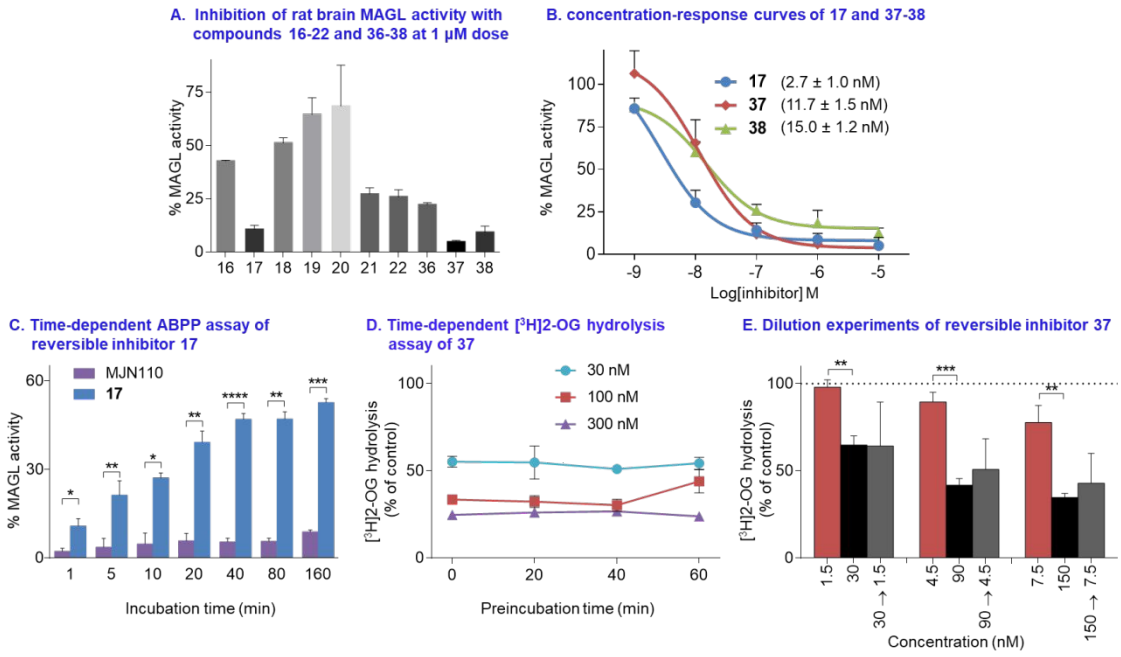

Figure 3. Inhibition properties of MAGL activity by compounds **18-22** and **36-38**. (A) Rat brain MAGL activity in the presence of compounds **16-22** and **36-38** at 1 μM concentration determined by ABPP assay; (B) Concentration-response curves of **17** and **37-38** for inhibition of rat brain MAGL activity determined by ABPP assay with pristimerin, a known reversible MAGL inhibitor, as reference (**Figure S3** in the Supporting Information); (C) MAGL activity determined at different incubation time points with **17** and the irreversible inhibitor MJN110 as control. Recovered MAGL activity over time indicates the binding of

compound **17** is reversible while the irreversible inhibitor MJN110 shows no significant time-dependent changes. (D) Time-dependent inhibition of [^{3}H]2-OG hydrolysis at three different concentrations of compound **37** (30, 100 and 300 nM). (E) Inhibition of 0.5 μM [^{3}H]2-OG hydrolysis by compound **37** without preincubation (red and black bars) or with 60 min of preincubation followed by dilution to reduce the free concentration 20-fold (gray bar). Given that this compound showed no time-dependence towards inhibition of [^{3}H]2-OG hydrolysis (data not shown), the data are consistent with a tight-binding but reversible inhibitor. All data are mean ± SD, n = 3-5. *p < 0.05, **p ≤0.01, and ***p ≤0.001.

As shown in **Table 2**, the selectivity of these three lead compounds **8**, **17** and **37** towards MAGL over FAAH was further investigated in ABPP assays, and none of them showed significant inhibition towards FAAH at a concentration up to 10 μM. In addition, for all three lead compounds, no significant interactions were observed with CB_1 and CB_2 receptors (up to a concentration of 30 μM, **Figure 4**) as well as ABHD6 and ABHD12 (up to a concentration of 10 μM), both of which also belong to serine hydrolase superfamily and play a vital role in the metabolism of 2-AG in the brain.

Lipophilicity of candidate compounds is an essential factor for the prediction of BBB permeability with 1.0 to 3.5 as the favorable range.[53-55] By means of the 'shake flask method', namely liquid-liquid partition between PBS and *n*-octanol,[56] the Log*D* values of **8**, **17** and **37** were 1.90 ± 0.38, 3.35 ± 0.50 and 2.70 ± 0.04, respectively (n = 3) (**Table 1**). The topological polar surface areas (tPSA) for these compounds were determined by in silico prediction with ChemBioDraw Ultra 14.0, and all of them exhibited reasonable tPSA (**Table 2**), which, together with the lipophilicity results, indicated a high possibility of sufficient brain permeability.

Entry	FAAH[a]	ABHD6[a]	ABHD12[a]	CB_1[b]	CB_2[b]	log*D*[c]	tPSA[d]
8	< 30% activity at 1 and 10 μM of **8**, **17** and **37**	< 30% activity at 1 and 10 μM of **8**, **17** and **37** in ABHD6/12 ABPP assay		< 30% activity at 30 μM of **8**, **17** and **37** CB_1/CB_2 agonist and antagonist assay		1.90 ± 0.38	65.45
17						3.35 ± 0.50	65.45
37						2.70 ± 0.04	59.46

Table 2. Binding potency and physicochemical properties of compounds **8**, **17** and **37**. [a]Determined by ABPP assay on rat brain membrane (MJN110 as positive control); [b]Determined by CB_1/CB_2 agonist and antagonist assays (CP55940, rimonabant, and SR144528 as positive control in CB_1/CB_2 agonist assays, CB_1 antagonist assay, and CB_2 antagonist assay, respectively); [c]Measured by "shake-flask" method quantified by LC-MS/MS. [d]Topological polar surface area (tPSA) was calculated by ChemBioDraw Ultra 14.0.

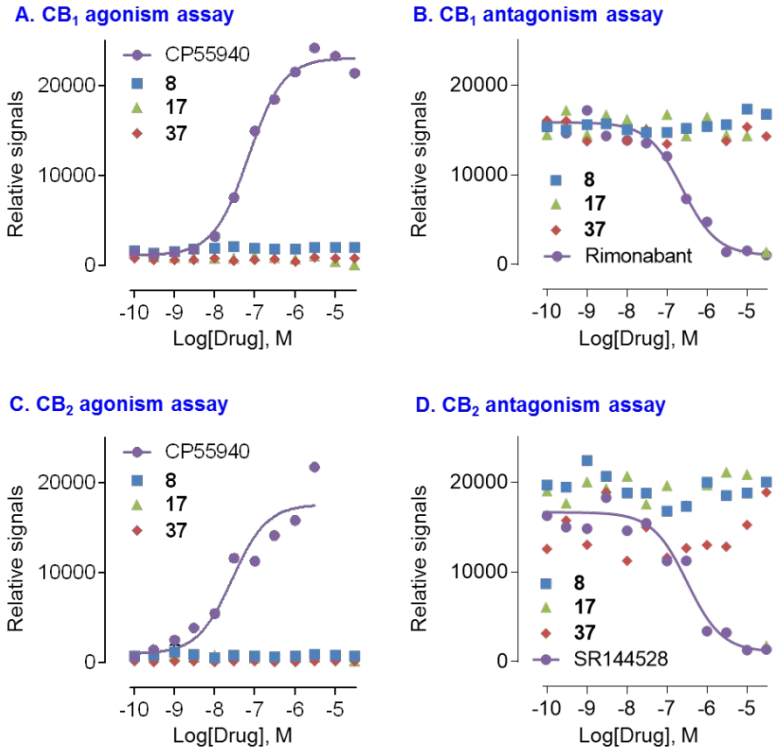

Figure 4. Pharmacological interactions of compounds **8**, **17** and **37** with CB_1/CB_2 receptors. (A) Agonism of **8**, **17** and **37** in the CB_1 assay with CP55940 as control; (B) Antagonism of **8**, **17** and **37** in the CB_1 assay with rimonabant as control; (C) Agonism of **8**, **17** and **37** in the CB_2 assay with CP55940 as control and (D) Antagonism of **8**, **17** and **37** in the CB_2 assay with SR144528 as control. All data are mean ± SD, n = 3-5.

Molecular docking studies. Based on the fact of excellent binding affinities for lead compounds **8**, **17** and **37** (0.88, 2.7, 11.7 nM, respectively), we then performed molecular docking studies with the purpose of identifying their possible interactions with MAGL and the corresponding binding domain (**Figure 5**). A 1.35-Å resolution crystal structure of a soluble form human monoglyceride lipase (MGLL) was downloaded (PDB ID: 3PE6) and its original ligand[57] was removed before performing the molecular docking studies. First, we reproduced the binding pose of the original ligand within 3PE6 using Autodock Vina, which yielded an excellent overlapping between the docked and original poses (**Figure S4**, Supporting Information). Subsequently, selected MAGL inhibitors **8, 17** and **37** were docked onto the 3PE6 structure (**Figure 5** and **Figure S5**, Supporting Information). As shown in **Figure 5A** and **5B**, both compounds **8** and **17** entered the 2-AG binding pocket and were located near the catalytic triad site, formed by Ser122, His269 and Asp239. Since the catalytic triad is essential for catalyzing 2-AG hydrolysis, compounds **8** and **17** reduced the accessibility of the active site to 2-AG, therefore inhibiting the 2-AG hydrolysis. Meanwhile, compound **37** was only partially docked into the 2-AG binding pocket, which blocked the "lid" of the pocket and prevented the 2-AG substrate from accessing the catalytic site (**Figure 5C**). It is also worth mentioning that although the Vina docking studies suggested that the docked pose of **37** did not bind to the oxyanionic hole or **37** was situated in a different binding pocket, more in-depth computational studies, including molecular dynamic simulation, are necessary to verify this hypothesis. Inside the binding pocket, we found π-π stacking interactions and hydrogen bonds. The π-π stackings were observed between the phenyl group of compounds **17**, **37** and nearby Phe159 side chains (**Figures 5B** and **5C**). And the Hydrogen bonds were found between compound **8** and Ala51 (**Figure 5A**), and also between compound **17** and nearby Ala51 and Met123

(**Figure 5B**). Overall, these docking results provided supportive evidence for the inhibitory mechanism of aforementioned compounds.

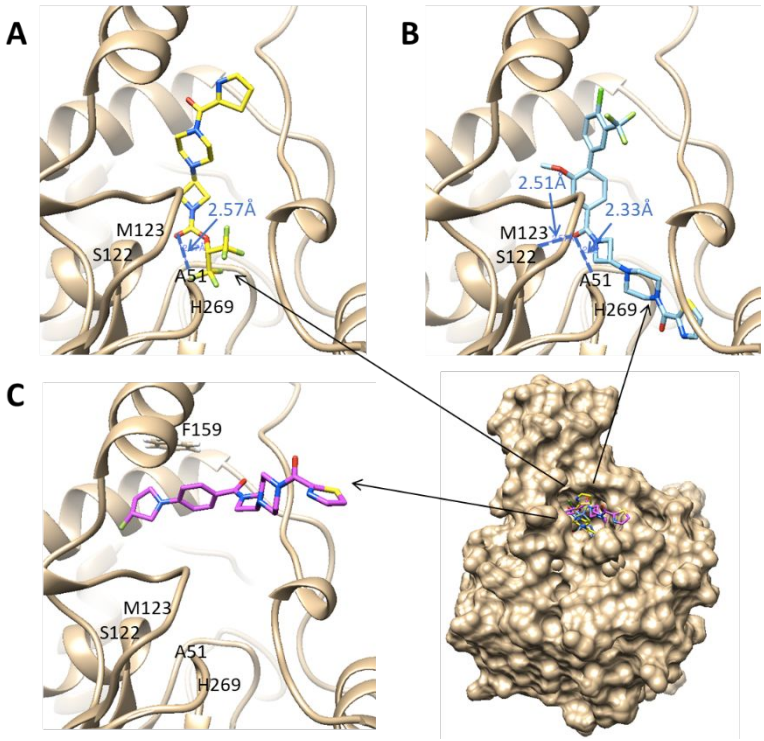

Figure 5. Molecular docking structures of compounds **8** (yellow in A; pre-covalent docking state), **17** (blue in B) and **37** (magenta in C) onto MAGL. The catalytic triad was labeled as Asp239, His269 and Ser122. Hydrogen-bonds between compounds and the MAGL protein were connected with solid lines. The bottom-right insets at each panel showed the docking pose of each compound into (or at the opening end of) the 2-AG binding pocket. The PDB ID of the protein structure is 3PE6.

Radiochemistry. The encouraging results of pharmacology and physiochemical property and docking studies prompted us to perform radiolabeling of **8**, **17** and **37** with carbon-11 or fluorine-18. In the case of **37**, we used its racemic form for preliminary proof-of-concept studies for brain permeability and binding specificity. The significance of labeling site selection in irreversible serine hydrolase PET tracers has been demonstrated by Wilson[58, 59] and our group.[39, 41] Therefore, for irreversible lead compound **8**, we utilized two ^{11}C-carbonylation approaches with [^{11}C]$COCl_2$ and [^{11}C]CO_2, respectively

(**Scheme 4A**). The piperazinyl azetidine precursor **7** for ^{11}C-carbonylation was synthesized as per the method depicted in **Scheme 1**. Initial radiosynthesis of **48** ([^{11}C]**8**) was performed with [^{11}C]$COCl_2$ generated from our previously reported procedure.[39] Reaction of [^{11}C]$COCl_2$ with 1,1,1,3,3,3-hexafluoro-2-propanol (HFIP) facilitated by 1,2,2,6,6-pentamethylpiperidine (PMP) followed by addition of azetidine **7** smoothly occurred to deliver ^{11}C-labeled carbamate **48** in an average 18% (*n* = 6) radiochemical yield (RCY) relative to starting [^{11}C]CO_2 (decay corrected). The radiochemical purity was ≥99% and the molar activity was 30–52 GBq/μmol (0.81–1.40 Ci/μmol). Alternative radiosynthesis of **48** was carried out based on our previously reported 'in-loop' [^{11}C]CO_2 fixation method.[60] Treatment of [^{11}C]CO_2 with 2-*tert*-butylimino-2-diethylamino-1,3-dimethylperhydro-1,3,2-diazaphosphorine (BEMP) and piperazinyl azetidine **7**, followed by successive addition of HFIP and phosphorus(V) oxychloride ($POCl_3$) in acetonitrile (MeCN), readily produced **48** in an average 2.5% decay-corrected RCY based on starting [^{11}C]CO_2 at the end-of-synthesis. The radiochemical purity was greater than 99% (*n* = 2) and the molar activity was as high as 288.6 GBq/μmol (7.8 Ci/μmol).

For lead compounds **17** and **37** with a reversible binding mechanism, we deployed two distinct labeling methods, namely ^{11}C-methylation of phenolic precursor **44** for lead compound **17** and ^{18}F-fluorination of mesylate precursor **47** for lead compound **37**, respectively (**Scheme 4B** and **4C**). The general procedure for preparation of precursors **44** and **47** was outlined in **Scheme 3A** and **3B**, respectively. Specifically, synthesis of phenolic precursor **44** commenced with the protection of phenol derivative **39** with chloromethyl methyl ether (MOMCl) to give bromobenzene derivative **40** in 90% yield. Subsequently, $Pd(PPh_3)_4$-catalyzed cross-coupling reaction of **40** with (4-chloro-3-(trifluoromethyl)phenyl)boronic acid **41**, followed by LiOH-triggered hydrolysis of the ester group, readily proceeded to give [1,1'-biphenyl]-4-carboxylic acid **42** in 89% yield over two steps. Coupling

of **42** with piperazinyl azetidine **7** in the presence of HOBT and EDC occurred to deliver azetidine amide **43** in 24% yield. The following deprotection of the methoxylmethyl ether (MOM) group from **43** was achieved with 6 *N* HCl, thus affording the desired phenolic precursor **44** in 80% yield. On the other hand, the synthetic route to mesylate precursor **47** involved a K_2CO_3 promoted displacement of ethyl 4-fluorobenzoate **23** by pyrrolidin-3-ol hydrochloride, followed by LiOH-mediated hydrolysis of the ester group, thus producing 4-(3-hydroxypyrrolidin-1-yl)benzoic acid **45** in 77% overall yield. Coupling of **45** with piperazinyl azetidine **7**, EDC and HOBT led to the isolation of hydroxyl-containing azetidine amide **46**, which was subsequently protected with methanesulfonyl chloride (MsCl) to generate the desired mesylate precursor **47** in 16% yield over two steps. As shown in **Scheme 4B**, the radiotracer **49** ([^{11}C]**17**) with reversible binding mechanism was prepared by reacting the phenolic precursor **44** with [^{11}C]CH_3I in 25% decay-corrected RCY based on starting [^{11}C]CO_2 at the end of synthesis with molar activity greater than 97.5 GBq/μmol. The ^{18}F-labeled radiotracer **50** ([^{18}F]**37**) was obtained by reacting the mesylate precursor **47** with [^{18}F]fluoride in the presence of K_2CO_3 and 4,7,13,16,21,24-hexaoxa-1,10-diazabicyclo[8,8,8]hexacosane (Kryptofix222) in an average RCY of 39% (decay corrected) with high radiochemical purity (>99%) and excellent molar activity (>110 GBq/μmol). All these radiotracers exhibited excellent in vitro stability without radiolysis up to 90 min after formulation. The efficient radiosynthesis, as well as excellent radiochemical purity and molar activity of **48**-**50** paved the way for subsequent in vivo investigation.

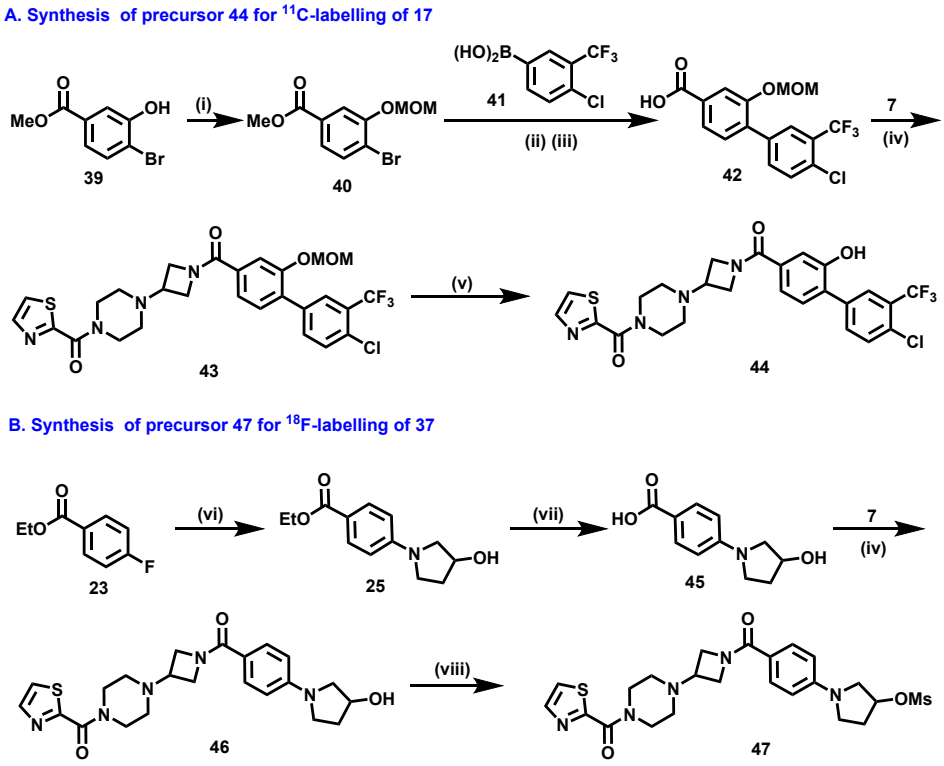

Scheme 3. Synthesis of labeling precursors **44** and **47** for MAGL PET tracers. Conditions: (i) MOMCl, K_2CO_3, acetone, rt, overnight; 95% yield; (ii) Pd $(PPh_3)_4$, K_2CO_3, toluene/H_2O, reflux, overnight; then (iii) LiOH, THF/H_2O, rt, overnight; 90% yield over two steps; (iv) HOBT, EDC•HCl, Et_3N, DMF, rt, 12 h; 24% yield for **43**; 22% yield for **46**; (v) 6 *N* HCl, MeOH, 66 °C, 2 h; 80% yield; (vi) pyrrolidin-3-ol hydrochloride, K_2CO_3, DMSO, 120 °C, 24 h; 79% yield; (vii) LiOH, THF/MeOH/H_2O, 40 °C, overnight; 97% yield; (viii) MsCl, Et_3N, CH_2Cl_2, rt, overnight; 70% yield; HOBT = 1-hydroxybenzotriazole hydrate; EDC•HCl = *N*-(3-Dimethylaminopropyl)-*N*′-ethylcarbodiimide hydrochloride; DMF = *N*,*N*-dimethylformamide; DMSO = methyl sulfoxide; MsCl = methanesulfonyl chloride.

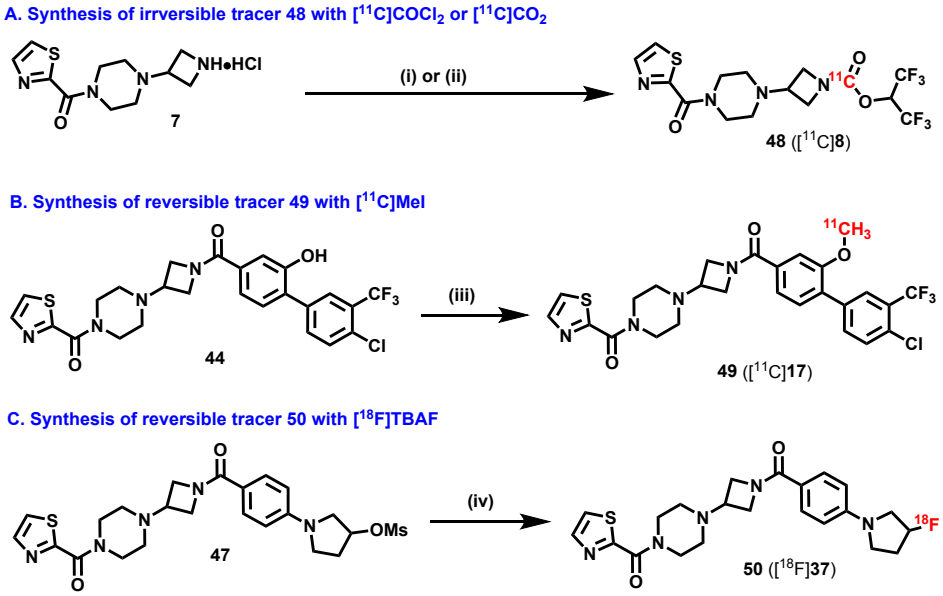

Scheme 4. Radiosynthesis of tracers **48-50**. Conditions: (i) [^{11}C]$COCl_2$, HFIP, PMP, THF; 30 °C, 1 min. 18% decay-corrected RCY (ii) [^{11}C]CO_2, BEMP, HFIP, $POCl_3$, rt, 1 min. 2.5% decay-corrected RCY; (iii) [^{11}C]MeI, NaOH, DMF, 70 °C, 5 min, 25% decay-corrected RCY; (iv) [^{18}F]KF, DMSO, 120 °C, 10 min, 39% decay-corrected RCY. HFIP = 1,1,1,3,3,3-hexafluoro-2-propanol; PMP = 1,2,2,6,6-pentamethylpiperidine; BEMP = 2-*tert*-butylimino-2-diethylamino-1,3-dimethylperhydro-1,3,2-diazaphosphorine.

Preliminary PET imaging studies of irreversible MAGL tracer 48 ([^{11}C]**8**). Dynamic PET acquisitions of radioligand **48** were carried out in Sprague-Dawley rats for 90 mins. Representative PET images in the brain (sagittal and coronal, summed images 0-90 min) and time-activity curves are shown in **Figure 6** and **Figure S6** in the Supporting Information. Compound **48** demonstrated excellent BBB penetration with maximum standard uptake value (SUV) of 2.26 at 3.5 min in the whole brain, and heterogeneous distribution with high uptake in cerebellum, striatum and hippocampus and low uptake in pons (**Figure 6A** and **Figure S6**, Supporting Information). No significant washout (ratio of $SUV_{3.5\ min}$ / $SUV_{90\ min}$ = 1.2) was observed during PET scans, which was aligned with characteristic plateaued time−activity curves of typically irreversible binding PET tracers.[40, 58, 61] Pretreatment with KML29 (3

mg/kg), a widely-used MAGL inhibitor, remarkably decreased the uptake of **48** in various brain regions and the whole brain uptake (~50% reduction based on area under curve, AUC), which demonstrated excellent in vivo specificity of **48** towards MAGL (**Figure 6B** and **Figure S6**). We then investigated the uptake, biodistribution and clearance of **48** by whole body distribution in mice at five time points (1, 5, 15, 30 and 60 min) after tracer injection (**Figure 6C** and **Table S1**, Supporting Information). Several organs including liver, adrenal glands, kidney and brown adipose tissue (BAT) exhibited high radioactivity levels at 30 min (>5% ID/g, injected dose per gram of wet tissue), which is consistent with the expression of MAGL in rodents.[62] The radioactivity levels in heart and lungs reached a plateau at 5 min, followed by slow washout. These results together with high activity remaining in the kidneys, liver, and small intestine suggested urinary and hepatobiliary elimination of **48**. To investigate the in vivo stability of **48**, we carried out radiometabolic analysis at 30 min post-injection of the radiotracers in mouse brain homogenate for **48**. The fraction of remaining parent **48** was determined to be 96% by radioHPLC, indicating excellent in vivo stability in the brain.

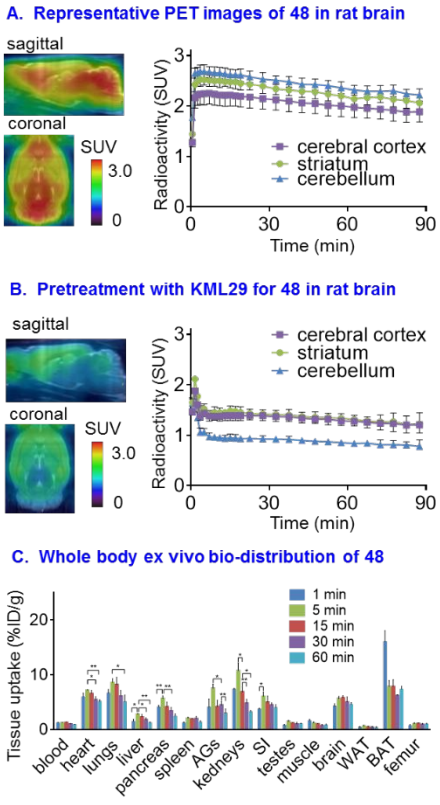

Figure 6. Representative PET images and time-activity curves of **48** in rat brain: (A) Baseline; (B) Blocking studies with KML29 (3 mg/kg); (C) Whole body ex vivo biodistribution studies. The brain uptake was measured and quantified by the standardized uptake value (SUV). Asterisks indicate statistical significance. $^{*}p < 0.05$, $^{**}p \leq 0.01$, and $^{***}p \leq 0.001$. AGs = adrenal glands; SI = small intestine; WAT = white adipose tissue; BAT = brown adipose tissue.

Preliminary PET imaging studies of reversible MAGL tracers 49 ([^{11}C]**17**) and **50** ([^{18}F]**37**). Dynamic PET acquisitions of reversible radioligands **49** and **50** were also performed in Sprague-Dawley rats for 90 mins, and both exhibited insufficient BBB permeability in rats (ca. 0.4 and 0.3 SUV, respectively, **Figure 7A-B** and **8A-B**). High levels of radioactivity were observed in brown adipose tissue (BAT), kidneys and liver (**Figure 7A** and **8A**), which is consistent with the expression of MAGL in periphery and confirmed by subsequent ex vivo biodistribution studies (**Figure 7C**, **8C** and **Table S2**, **S3**, Supporting Information).[62] In contrast to the irreversible radioligand **48**, both **49** and **50**

exhibited initial high uptake (> 15% ID/g at 1 min) in heart and lungs followed by fast clearance (ratio of %ID/g $_{1\ min/60\ min}$ in heart: 3.49 for **49**, 6.34 for **50**; ratio of %ID/g$_{1\ min/60\ min}$ in lungs: 6.80 for **49**, 10.38 for **50**). Besides, the radioactivity of **49** and **50** were also rapidly washed out from blood with the $SUV_{1\ min}$ / $SUV_{60\ min}$ ratios to be 5.1 and 3.5, respectively. These results together with high bound activity in the kidneys, liver, and small intestine suggested fast urinary and hepatobiliary elimination of **49** and **50**. To test the in vivo specificity of **49** and **50** towards MAGL, we carried out blocking experiments by pre-treatment of KML29 (3 mg/kg). While **50** exhibited significant blocking effect in two MAGL-rich organs including adrenal glands (80%) and BAT (88%), **49** demonstrated comparable result in BAT (63% decrease), and no statistical significance was observed for the uptake in adrenal glands (13% decrease) between the baseline and blocking conditions (**Figure 7D** and **8D**). The increased level of non-specific binding of compound **49** in adrenal glands and BAT was likely attributed to its higher lipophilicity. In tissues with low MAGL expression, such as lungs and muscle, no obvious contrast was observed for both **49** and **50** between baseline and blocking conditions, indicating a limited window to show specific binding in MAGL-deficient organs. Furthermore, in MAGL-deficient organs such as lungs and muscle, no significant changes of uptake were observed for both **49** and **50**. The peripherally-restricted distribution of **49** and **50** may be attributed to their interaction with P-glycoprotein (Pgp) and breast cancer resistance protein (Bcrp), both of which are crucial components of ATP-binding cassette (ABC) efflux transporter family co-localizing at the BBB. To verify this hypothesis, we conducted PET imaging studies of **49** and **50** in wild-type and Pgp/Bcrp knockout (ABCB1a/1b-/-ABCG2-/-) mice. As outlined in **Figure 7E-F** and **8E-F**, the brain uptake was significantly increased in Pgp/Bcrp knockout mice than that of wide-type mice, and reached a plateau of 1.4 SUV at 2.5 min for **49** and 1.0 SUV at 11 min for **50**, respectively. These results demonstrated that **49** and **50** had intensive interactions with

ABC efflux transporters at the BBB including Pgp and Bcrp, which may explain their limited brain accumulation at tracer dose. The extensive interactions of **49** and **50** with ABC efflux transporters are probably attributed to the nature that they are nitrogenous compounds and characterized by one or more positive charges in the physiological conditions. To investigate the in vivo stability of **49** and **50**, we performed radiometabolic analysis at 30 min post-injection of the radiotracers in mouse plasma homogenate. The fractions of parent **49** and **50** were determined by radioHPLC to be 62% and 45%, respectively, indicating reasonable metabolic stability.

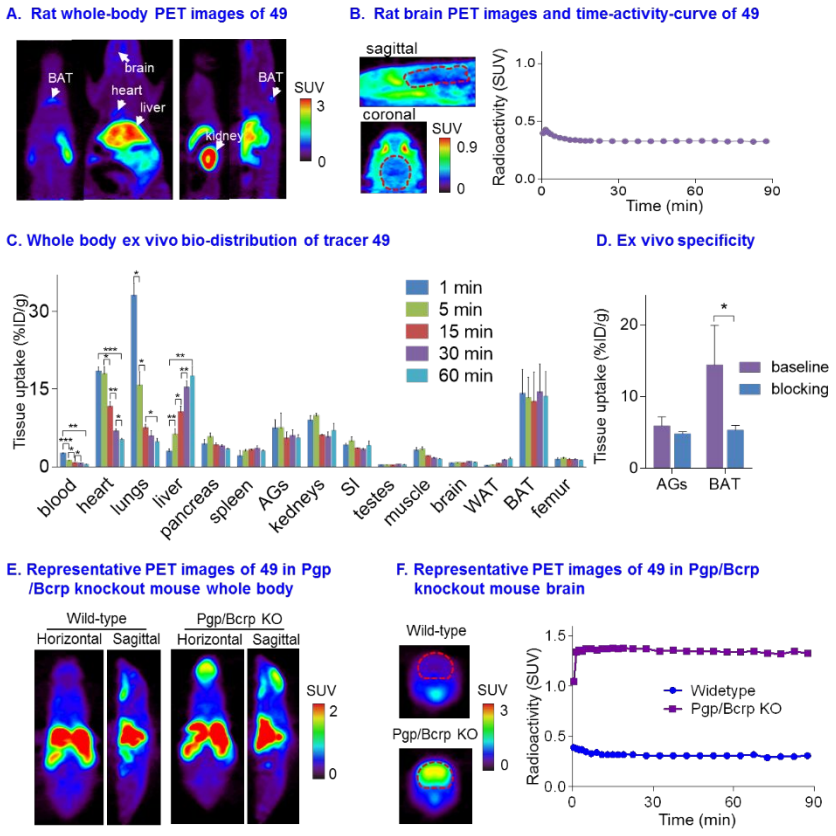

Figure 7. Representative PET images and time-activity curves of **49**: (A) Baseline PET images in SD rat (summed 0-90 min); (B) Baseline PET images (summed 0-90 min) and time-activity curve of **49** in rat brain; (C) Whole body ex vivo biodistribution in mice at five different time points (1, 5, 15, 30 and 60 min) post injection of **49**. All data are mean ± SD, n = 4. (D) ex vivo Specificity measured by the uptake of **49** in MAGL-rich tissues adrenal glands and brown adipose tissue (baseline and blocking

with KML29 (3 mg/kg)); (E) Representative PET images of wild-type and Pgp/Bcrp knockout mouse (summed 0-90 min); (F) Representative PET images and time-activity curve of **49** of wild-type and Pgp/Bcrp knockout mouse (summed 0-90 min). Asterisks indicate statistical significance. $^{*}p < 0.05$, $^{**}p \leq 0.01$, and $^{***}p \leq 0.001$. AGs = adrenal glands; SI = small intestine; WAT = white adipose tissue; BAT = brown adipose tissue.

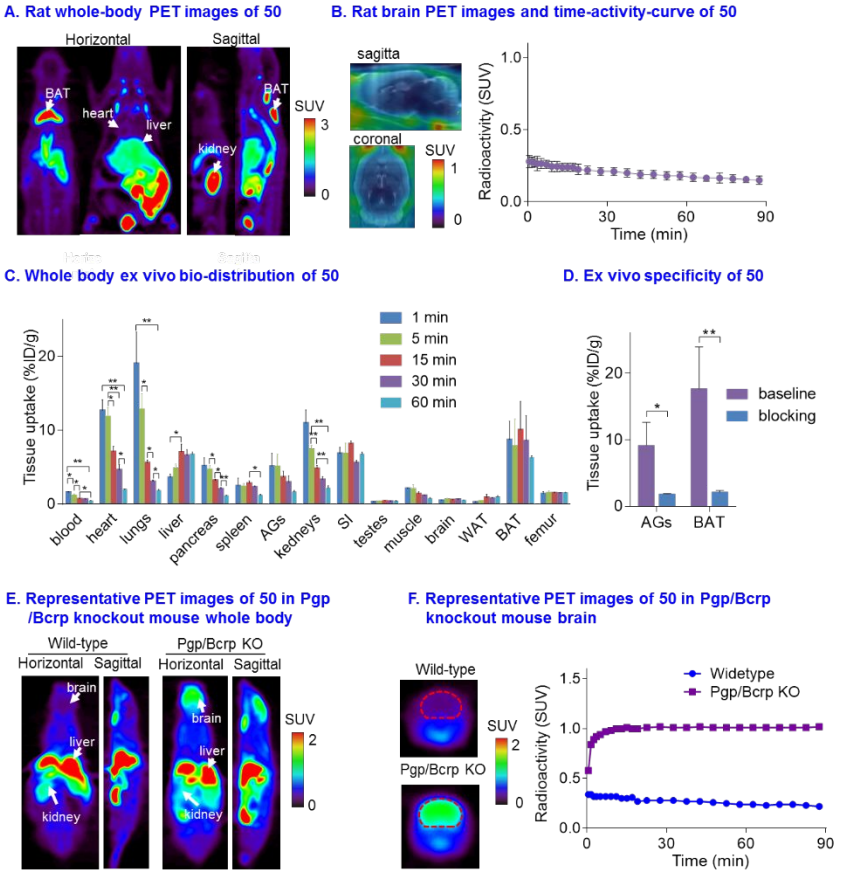

Figure 8. Representative PET images and time-activity curves of **50**. (A) Baseline PET images in SD rat (summed 0-90 min); (B) Baseline PET images (summed 0-90 min) and time-activity curve of **50** in rat brain; (C) Whole body *ex vivo* biodistribution in mice at five different time points (1, 5, 15, 30 and 60 min) post injection of **50**. All data are mean ± SD, n = 4; (D) *ex vivo* Specificity measured by the uptake of **50** in MAGL-rich tissues including adrenal glands (AGs) and brown adipose tissue (BAT) (baseline and blocking with KML29 (3 mg/kg)); (E) Representative PET images of wild-type and Pgp/Bcrp knockout mouse (summed 0-90 min); (F) Representative PET images and time-activity curve of **50** of wild-type and Pgp/Bcrp knockout

mouse (summed 0-90 min). Asterisks indicate statistical significance. $^{*}p < 0.05$, $^{**}p \leq 0.01$, and $^{***}p \leq 0.001$. AGs = adrenal glands; SI = small intestine; WAT = white adipose tissue; BAT = brown adipose tissue.

CONCLUSION

We have established a focused library of MAGL inhibitors with irreversible or reversible binding mechanisms by the utilization of a tail switching strategy on a piperazinyl azetidine scaffold. Potency, selectivity as well as irreversible or reversible binding profiles were determined in vitro by two different tissue-based assays, namely [^{3}H]2-OG hydrolysis and ABPP. Lipophilicity (Log*D*) of candidate compounds was also measured by the "shake-flask" method to estimate the brain permeability. As a result, compound **8** was identified as the most promising irreversible MAGL inhibitor, and compounds **17** and **37** were identified as the most promising reversible inhibitors. Possible molecular interactions between these lead compounds and MAGL, as well as the corresponding binding domain were also identified through molecular docking studies. The corresponding ^{11}C- and ^{18}F-isotopologues **48** ([^{11}C]**8**; also known as [^{11}C]MAGL-2-11), **49** ([^{11}C]**17**; also known as [^{11}C]PAD) and **50** ([^{11}C]**37**; also known as [^{18}F]MAGL-4-11) were synthesized in excellent radiochemical yield, high molar activity and high radiochemical purity, and with diverse radiolabeling strategies, including [^{11}C]$COCl_2$ cyclization, in-loop [^{11}C]CO_2 fixation, ^{11}C-methylation and ^{18}F-fluorination. The pharmacokinetic profiles of these radioligands including brain uptake, clearance and binding specificity were further investigated by PET imaging and ex vivo whole-body distribution studies in rodents. The irreversible tracer **48** demonstrated excellent BBB penetration and heterogenous regional brain uptake and high binding specificity, which was in line with MAGL distribution. The reversible tracers **49** and **50** showed limited brain uptake, but exhibited excellent binding specificity towards MAGL in the periphery as evidenced by ex vivo

blocking bio-distribution studies. We also performed PET experiments in Pgp/Bcrp knockout mice, in which **49** and **50** exhibited substantially increased activity accumulation in the brain, indicating that the underlying cause of their limited brain uptake was probably attributed to the significant interaction with ABC efflux transporters. Therefore, further optimization is necessary to increase brain permeability by minimizing the interaction with Pgp/Bcrp efflux transporters, and further validation in comprehensive in vivo MAGL inhibitory experiments is also desirable to evaluate the therapeutic potential of these novel molecules. Multiparameter optimization (MPO), namely the approach to simultaneously optimize and balance basicity (pKa), lipophilicity (clogP and clogD), number of hydrogen bond donors (HBD), polar surface area (tPSA) and molecular weight (MW), has demonstrated its usefulness in the improvement of molecular properties and ADME profile, including brain penetration.[42, 63-66] We will utilize this strategy to design next-generation brain penetrant radioligands for reversible binding mechanism. In conclusion, this work not only provides the first synergetic medicinal chemistry approach to both irreversible and reversible MAGL inhibitors based on a unique piperazinyl azetidine scaffold, but also paves the way towards the development of next generation reversible PET tracers for translational PET imaging studies.

EXPERIMENTAL SECTION

General consideration. The general procedure for experimental section was described previously[41] with minor modification in this work. All the chemicals employed in the synthesis were purchased from commercial vendors and used without further purification. Thin-layer chromatography (TLC) was conducted with 0.25 mm silica gel plates ($^{60}F_{254}$) and visualized by exposure to UV light (254 nm) or stained with potassium permanganate. Flash column chromatography was performed using silica gel

(particle size 0.040-0.063 mm). Nuclear magnetic resonance (NMR) spectra were obtained either on a Bruker spectrometer 300 MHz. Chemical shifts (δ) are reported in ppm, and coupling constants are reported in Hertz. The multiplicities are abbreviated as follows: s = singlet, d = doublet, t = triplet, q = quartet, quint = quintet, sext = sextet, sept = setpet, m = multiplet, br = broad signal, dd = doublet of doublets. For mass spectrometer measurement, the ionization method is ESI using Agilent 6430 Triple Quad LC/MS. Lipophilicity was calculated by ChemBioDraw Ultra 14.0 (CambridgeSoft Corporation, PerkinElmer, USA). All tested MAGL inhibitors showed high purity (≥95%) as determined by a reverse-phase HPLC (Gemini ® 5 μm, NX-C18 110 Å column (3 mm ID × 150 mm). The lead compounds **8**, **17** and **37** did not show any promiscuous moieties in the Pan Assay Interference Compounds Assay (PAINS) using two different in silico filters (http://www.swissadme.ch/index.php and http://zinc15.docking.org/patterns/home/).[67] Molar activity determinations are reported at the end of synthesis, unless otherwise stated. The animal experiments were approved by the Institutional Animal Care and Use Committee of Massachusetts General Hospital or the Animal Ethics Committee at the National Institutes for Quantum and Radiological Science and Technology, National Institute of Radiological Sciences. CD-1 mice (female; 7 weeks, 22-24 g), DdY mice (male; 7 weeks, 34-36 g), Sprague-Dawley rats (male; 7 weeks; 210-230 g) were kept on a 12 h light/12 h dark cycle and were allowed food and water *ad libitum*. Male Pgp/Bcrp knockout (Mdr1a/1b(-/-) and Abcg(-/-)) miceand male wild-type mice (FVB) were purchased from Taconic (Hudson, NY).

Chemistry.

General procedure for synthesis of 1,1,1,3,3,3-hexafluoropropan-2-yl 3-(4-(thiazole-2-carbonyl)piperazin-1-yl)azetidine-1-carboxylate (**8)**. Under nitrogen atmosphere, a solution of 4-

nitrophenyl chloroformate (201.6 mg, 1.0 mmol) in CH_2Cl_2 (2.5 mL) was added dropwise to a solution of 1,1,1,3,3,3-hexafluoro-2-propanol (420.2 mg, 2.5 mmol), pyridine (197.8 mg, 2.5 mmol) and 4-dimethylaminopyridine (DMAP, 12.3 mg, 0.1 mmol) in CH_2Cl_2 (2.5 mL) at 0 °C. The resulting mixture was stirred at room temperature overnight, followed by addition of **7** (303.2 mg, 1.05 mmol) and Et_3N (404.8 mg, 4.0 mmol) in CH_2Cl_2 (4.0 mL). The reaction mixture was stirred at room temperature for 5 h, then evaporated under reduced pressure to dryness and re-dissolved in ethyl acetate (25 mL). After successively washed with H_2O, 1 M aqueous potassium carbonate solution and brine, the organic phase was dried over $MgSO_4$, and evaporated to dryness. The residue was purified by silica column chromatography (PE/EA = 3/1) to give product **8** as a white solid in 20% yield. Melting point: 102 – 103 ºC. ^{1}H NMR (300 MHz, $CDCl_3$) δ 7.87 (d, *J* = 3.2 Hz, 1H), 7.54 (d, *J* = 3.2 Hz, 1H), 5.75 – 5.54 (m, 1H), 4.48 (s, 2H), 4.20 – 3.97 (m, 4H), 3.86 – 3.84 (m, 2H), 3.35 – 3.16 (m, 1H), 2.48 – 2.46 (m, 4H); ^{19}F NMR (282 MHz, $CDCl_3$) δ -69.74 (d); ^{13}C NMR (75 MHz, $CDCl_3$) δ 165.06, 159.34, 151.89, 143.35, 124.42, 120.79 (d, *J* = 281.9 Hz), 68.76 – 66.88 (m), 54.23, 54.09, 53.35, 50.18, 49.60, 46.02, 43.08. **HRMS** (ESI): *m/z* calculated for $C_{15}H_{16}F_6N_4O_3SNa^+$ $[M + Na]^+$: 469.0740, found: 469.0739.

General procedure for synthesis of 2,2,2-trifluoroethyl 3-(4-(thiazole-2-carbonyl)piperazin-1-yl) azetidine-1-carboxylate (9). A solution of triphosgene (0.2 mmol) in dichloromethane (DCM, 0.5 mL) was added dropwise to a solution of CF_3CH_2OH (0.6 mmol) and Et_3N (0.6 mmol) in DCM (1 mL) at 0 °C. The mixture was stirred at room temperature for 4 hours, followed by the addition of **7** (0.5 mmol) and a solution of Et_3N (2 mmol) in DCM (2 mL). After stirring at room temperature for 4 hours, the mixture was evaporated to dryness and re-dissolved in ethyl acetate (10 mL). The organic phase was washed with H_2O (10 mL) and the aqueous phase was extracted with ethyl acetate (10 mL x 2). The combined organic layers were washed with brine (20 mL), dried over Na_2SO_4, and concentrated

under reduced pressure. The residue was purified by silica column chromatography (eluent: ethyl acetate) to give product **9** as a white solid in 43% yield. Melting point: 95 – 97 °C. ^{1}H NMR (300 MHz, $CDCl_3$) δ 7.85 (s, 1H), 7.52 (s, 1H), 4.54–4.32 (m, 4H), 4.14–3.76 (m, 6H), 3.25–3.13 (m, 1H), 2.44 (s, 4H); ^{19}F NMR (282 MHz, $CDCl_3$) δ -70.36 (t, *J* = 8.4 Hz); ^{13}C NMR (75 MHz, $CDCl_3$) δ 164.90, 159.11, 153.99, 143.11, 124.15, 123.02 (q, *J* = 277.4 Hz), 60.91 (q, *J* = 36.4 Hz), 53.99, 53.65, 52.93, 49.96, 49.36, 45.89, 42.94. **HRMS** (ESI): *m/z* calculated for $C_{14}H_{17}F_3N_4O_3SNa^+$ $[M + Na]^+$: 401.0866, found: 401.0867.

Preparation of (4-(1-(1*H*-1,2,4-triazole-1-carbonyl)azetidin-3-yl) piperazin-1-yl) (thiazol-2-yl) methanone (10). Compound **10** was prepared in a manner similar to that described for **9** in 28% yield as a white solid. Melting point: 164 – 165 °C. ^{1}H NMR (300 MHz, $CDCl_3$) δ 8.88 (s, 1H), 7.97 (s, 1H), 7.87 (d, *J* = 3.2 Hz, 1H), 7.54 (d, *J* = 3.2 Hz, 1H), 4.82 – 4.65 (m, 1H), 4.62 – 4.39 (m, 3H), 4.33 – 4.20 (m, 1H), 4.16 – 4.05 (m, 1H), 3.85 (s, 2H), 3.34 – 3.19 (m, 1H), 2.50 (t, *J* = 4.9 Hz, 4H); ^{13}C NMR (75 MHz, $CDCl_3$) δ 165.09, 159.33, 153.01, 147.62, 144.92, 143.32, 124.38, 58.86, 54.62, 53.23, 50.23, 49.64, 46.10, 43.17. **HRMS** (ESI): *m/z* calculated for $C_{14}H_{17}N_7O_2SNa^+$ $[M + Na]^+$: 370.1057, found: 370.1059.

Preparation of (4-(1-(1*H*-benzo[*d*][1,2,3]triazole-1-carbonyl) azetidin-3-yl)piperazin-1-yl) (thiazol-2-yl)methanone (11). Compound **11** was prepared in a manner similar to that described for **9** in 7% yield as a white solid. Melting point: 218 – 219 °C. ^{1}H NMR (300 MHz, $CDCl_3$) δ 8.26 (dt, *J* = 8.4, 0.9 Hz, 1H), 8.08 (dt, *J* = 8.3, 0.9 Hz, 1H), 7.88 (d, *J* = 3.2 Hz, 1H), 7.60 (ddd, *J* = 8.3, 7.1, 1.1 Hz, 1H), 7.54 (d, *J* = 3.2 Hz, 1H), 7.46 (ddd, *J* = 8.2, 7.1, 1.1 Hz, 1H), 4.86 (dd, *J* = 9.8, 7.5 Hz, 1H), 4.69 (dd, *J* = 10.2, 5.1 Hz, 1H), 4.51 (s, 2H), 4.43 – 4.31 (m, 1H), 4.23 (dd, *J* = 9.4, 4.6 Hz, 1H), 3.89 (s, 2H), 3.45 – 3.26 (m, 1H), 2.55 (d, *J* = 4.5 Hz, 4H); ^{13}C NMR (75 MHz, $CDCl_3$) δ 165.06, 159.40,

149.50, 145.24, 143.37, 132.48, 129.86, 125.68, 124.39, 119.91, 114.44, 59.30, 54.82, 53.33, 50.31, 49.72, 46.17, 43.22. **HRMS** (ESI): *m/z* calculated for $C_{18}H_{19}N_7O_2SNa^+$ $[M + Na]^+$: 420.1213, found: 420.1215.

General procedure for synthesis of 1,3-dioxoisoindolin-2-yl 3-(4-(thiazole-2-carbonyl)piperazin-1-yl) azetidine-1-carboxylate (12). A solution of Et_3N (0.84 mmol) in DCM (0.5 mL) was added dropwise to a solution of 2-hydroxyisoindoline-1,3-dione (0.7 mmol) and triphosgene (0.14 mmol) in DCM (1.5 mL) at 0 °C. The mixture was stirred at room temperature for 16 hours, followed by addition of **7** (0.5 mmol) and a solution of Et_3N (1 mmol) in DCM (1 mL). After stirring at room temperature for another 4 hours, the mixture was evaporated to dryness and re-dissolved in ethyl acetate (10 mL). The organic phase was washed with H_2O (10 mL) and the aqueous phase was extracted with ethyl acetate (10 mL x 2). The combined organic layers were washed with brine (20 mL), dried over Na_2SO_4, and concentrated under reduced pressure. The residue was purified by silica column chromatography (eluent: ethyl acetate) to give product **12** in 29% yield as a light yellow solid. Melting point: 180 – 182 °C. ^{1}H NMR (300 MHz, $CDCl_3$) δ 7.90 – 7.84 (m, 3H), 7.77 (dd, J = 5.5, 3.1 Hz, 2H), 7.55 (d, J = 3.2 Hz, 1H), 4.58 – 4.43 (m, 2H), 4.37 – 4.02 (m, 4H), 3.87 (s, 2H), 3.39 – 3.26 (m, 1H), 2.56 – 2.43 (m, 4H); ^{13}C NMR (75 MHz, $CDCl_3$) δ 165.00, 162.50, 159.28, 151.35, 143.28, 134.81, 129.00, 124.33, 124.00, 54.59, 54.43, 53.84, 50.01, 49.47, 46.06, 43.12. **HRMS** (ESI): *m/z* calculated for $C_{20}H_{19}N_5O_5SNa^+$ $[M + Na]^+$: 464.0999, found: 464.0998.

General procedure for synthesis of 2,5-dioxopyrrolidin-1-yl 3-(4-(thiazole-2-carbonyl) piperazin-1-yl) azetidine-1-carboxylate (13). Bis(2,5-dioxopyrrolidin-1-yl) carbonate (0.6 mmol) was added to a solution of (4-(azetidin-3-yl)piperazin-1-yl)(thiazol-2-yl)methanone hydrochloride **7** (0.5 mmol) and Et_3N (1 mmol) in DCM (2 mL). After stirring at ambient temperature for 5 hours, the

mixture was evaporated to dryness and re-dissolved in ethyl acetate (10 mL). The organic phase was washed with H_2O (10 mL) and then extracted with ethyl acetate (10 mL x 2). The combined organic layers were washed with brine (20 mL), dried over Na_2SO_4, and concentrated under reduced pressure. The residue was purified by silica column chromatography (eluent: ethyl acetate) to give product **13** in 14% yield as a white solid. Melting point: 209 – 211 °C. ^{1}H NMR (300 MHz, $CDCl_3$) δ 7.87 (s, 1H), 7.54 (s, 1H), 4.47 (s, 2H), 4.15 (dd, *J* = 38.7, 31.8 Hz, 4H), 3.84 (s, 2H), 3.30 (s, 1H), 2.81 (s, 4H), 2.46 (s, 4H); ^{13}C NMR (75 MHz, $CDCl_3$) δ 169.83, 165.03, 159.27, 150.52, 143.27, 124.33, 54.53, 53.77, 49.99, 49.45, 46.06, 43.11, 25.59. **HRMS** (ESI): *m/z* calculated for $C_{16}H_{19}N_5O_5SNa^+$ $[M + Na]^+$: 416.0999, found: 416.0997.

General procedure for synthesis of (4-(1-(2-methoxy-[1,1'-biphenyl]-4-carbonyl)azetidin-3-yl)piperazin-1-yl)(thiazol-2-yl)methanone (16). Under nitrogen atmosphere, a mixture of 2-methoxy-[1,1'-biphenyl]-4-carboxylic acid (182.6 mg, 0.8 mmol), **7** (277.3 mg, 0.96 mmol), 1-hydroxybenzotriazole (HOBT, 14% wet with H_2O, 326.8 mg, 2.08 mmol), *N*-(3-dimethylaminopropyl)-*N*-ethylcarbodiimide hydrochloride (EDC•HCl, 398.8 mg, 2.08 mmol) and Et_3N (647.6 mg, 6.4 mmol) in DMF (8 mL) was stirred at room temperature for 16 h. Then the mixture was poured into saturated aqueous $NaHCO_3$ solution, and extracted with ethyl acetate for 3 times. The combined organic layers were washed with brine, dried over anhydrous Na_2SO_4, and concentrated in vacuo. The residue was purified by silica column chromatography (PE/EA = 1/3) to give **16** as a white solid in 22% yield. Melting point: 92 – 93 °C. ^{1}H NMR (300 MHz, $CDCl_3$) δ 7.86 (d, *J* = 3.2 Hz, 1H), 7.54 – 7.48 (m, 3H), 7.45 – 7.37 (m, 2H), 7.37 – 7.29 (m, 3H), 7.22 – 7.17 (m, 1H), 4.53 – 4.10 (m, 6H), 3.96 – 3.76 (m, 5H), 3.32 – 3.17 (m, 1H), 2.50 (s, 4H); ^{13}C NMR (75 MHz, $CDCl_3$) δ 170.31, 165.01, 159.28, 156.74, 143.29, 137.67, 133.66, 133.30, 130.60, 129.54, 128.20, 127.58, 124.35, 120.12, 111.14, 57.29, 55.87,

54.42, 52.70, 50.24, 49.65, 46.00, 43.06. **HRMS** (ESI): *m/z* calculated for $C_{25}H_{26}N_4O_3SNa^+$ $[M + Na]^+$: 485.1618, found: 485.1619.

Preparation of (4-(1-(4'-chloro-2-methoxy-3'-(trifluoromethyl)-[1,1'-biphenyl]-4-carbonyl)azetidin-3-yl)piperazin-1-yl)(thiazol-2-yl)methanone (17). Compound **17** was prepared in a manner similar to that described for **16** in 25% yield as a white solid. Melting point: 82 – 83 ºC. ^{1}H NMR (300 MHz, $CDCl_3$) δ 7.86 (d, *J* = 3.2 Hz, 1H), 7.82 (d, *J* = 1.6 Hz, 1H), 7.66 – 7.60 (m, 1H), 7.57 – 7.49 (m, 2H), 7.35 – 7.33 (m, 1H), 7.28 (t, *J* = 7.3 Hz, 1H), 7.23 – 7.18 (m, 1H), 4.54 – 4.44 (m, 2H), 4.39 – 4.20 (m, 3H), 4.17 – 4.07 (m, 1H), 3.91 – 3.83 (m, 5H), 3.32 – 3.22 (m, 1H), 2.51 – 2.49 (m, 4H); ^{19}F NMR (282 MHz, $CDCl_3$) δ -58.52 (s); ^{13}C NMR (75 MHz, $CDCl_3$) δ 169.97, 165.03, 159.33, 156.66, 143.32, 136.59, 134.44, 133.91, 131.40 (q, *J* = 1.8 Hz), 131.26, 130.88, 130.35, 128.63 (q, *J* = 5.4 Hz), 128.24 (q, *J* = 31.3 Hz), 124.40, 123.03 (q, *J* = 273.3 Hz), 120.27, 111.32, 57.28, 55.96, 54.44, 52.79, 50.27, 49.68, 46.03, 43.09. **HRMS** (ESI): *m/z* calculated for $C_{26}H_{24}F_3N_4O_3SClNa^+$ $[M + Na]^+$: 587.1102, found: 587.1101.

Preparation of (4-(1-(3-methoxy-4-(pyridin-3-yl)benzoyl)azetidin-3-yl)piperazin-1-yl)(thiazol-2-yl)methanone (18). Compound **18** was prepared in a manner similar to that described for **16** in 28% yield as a white solid. Melting point: 90 – 91 ºC. ^{1}H NMR (300 MHz, $CDCl_3$) δ 8.71 (s, 1H), 8.52 (s, 1H), 7.83 – 7.81 (m, 2H), 7.51 – 7.49 (m, 1H), 7.32 – 7.16 (m, 4H), 4.48 – 4.20 (m, 5H), 4.10 – 4.06 (m, 1H), 3.81 (s, 5H), 3.24 – 3.20 (m, 1H), 2.45 (s, 4H); ^{13}C NMR (75 MHz, $CDCl_3$) δ 169.88, 164.84, 159.17, 156.75, 149.70, 148.05, 143.17, 137.07, 134.22, 133.49, 130.29, 129.65, 124.26, 123.10, 120.15, 111.08, 57.20, 55.78, 54.26, 52.68, 50.11, 49.51, 45.93, 42.98. **HRMS** (ESI): *m/z* calculated for $C_{24}H_{25}N_5O_3SNa^+$ $[M + Na]^+$: 486.1570, found: 486.1568.

Preparation of (4-(1-(3-methoxy-4-(pyridin-4-yl)benzoyl)azetidin-3-yl)piperazin-1-yl)(thiazol-2-yl)methanone (19). Compound **19** was prepared in a manner similar to that described for **16** in 23% yield as a white solid. Melting point: 85 – 86 ºC. ^{1}H NMR (300 MHz, $CDCl_3$) δ 8.64 – 8.62 (m, 2H), 7.85 (d, *J* = 3.1 Hz, 1H), 7.54 – 7.46 (m, 3H), 7.41 – 7.30 (m, 2H), 7.27 – 7.19 (m, 1H), 4.52 – 4.22 (m, 5H), 4.15 – 4.06 (m, 1H), 3.87 – 3.80 (m, 5H), 3.30 – 3.19 (m, 1H), 2.50 – 2.46 (m, 4H); ^{13}C NMR (75 MHz, $CDCl_3$) δ 169.84, 164.99, 159.29, 156.87, 149.05, 146.09, 143.28, 134.99, 130.31, 130.23, 124.46, 124.36, 120.22, 111.37, 57.27, 55.93, 54.39, 52.80, 50.23, 49.64, 46.04, 43.09. **HRMS** (ESI): *m/z* calculated for $C_{24}H_{25}N_5O_3SNa^+$ $[M + Na]^+$: 486.1570, found: 486.1571.

Preparation of (4-(1-(3-methoxy-4-(pyrimidin-5-yl)benzoyl)azetidin-3-yl)piperazin-1-yl)(thiazol-2-yl)methanone (20). Compound **20** was prepared in a manner similar to that described for **16** in 23% yield as a white solid. Melting point: 89 – 90 ºC. ^{1}H NMR (300 MHz, $CDCl_3$) δ 9.16 (s, 1H), 8.90 (s, 2H), 7.86 (d, *J* = 3.2 Hz, 1H), 7.53 (d, *J* = 3.2 Hz, 1H), 7.40 – 7.30 (m, 2H), 7.27 – 7.22 (m, 1H), 4.54 – 4.22 (m, 5H), 4.16 – 4.06 (m, 1H), 3.87 (s, 5H), 3.32 – 3.18 (m, 1H), 2.52 – 2.48 (m, 4H); ^{13}C NMR (75 MHz, $CDCl_3$) δ 169.73, 164.98, 159.31, 157.38, 156.95, 156.91, 143.31, 135.28, 131.51, 130.09, 126.22, 124.41, 120.42, 111.34, 57.23, 55.98, 54.42, 52.78, 50.25, 49.66, 45.94, 43.04. **HRMS** (ESI): *m/z* calculated for $C_{23}H_{24}N_6O_3SNa^+$ $[M + Na]^+$: 487.1523, found: 487.1526.

Preparation of (4-(1-(4-(furan-3-yl)-3-methoxybenzoyl)azetidin-3-yl)piperazin-1-yl)(thiazol-2-yl)methanone (21). Compound **21** was prepared in a manner similar to that described for **16** in 39% yield as a white solid. Melting point: 91 – 92 ºC. ^{1}H NMR (300 MHz, $CDCl_3$) δ 8.04 (d, *J* = 0.5 Hz, 1H), 7.85 (d, *J* = 3.2 Hz, 1H), 7.52 (d, *J* = 3.2 Hz, 1H), 7.51 – 7.43 (m, 2H), 7.31 (d, *J* = 1.0 Hz, 1H), 7.17 (dd, *J* = 7.9, 1.4 Hz, 1H), 6.80 – 6.76 (m, 1H), 4.47 (d, *J* = 19.2 Hz, 2H), 4.37 – 4.20 (m, 3H), 4.14 – 4.10 (m, *J* = 2.7 Hz, 1H), 3.94 (s, 3H), 3.90 – 3.81 (m, 2H), 3.29 – 3.20 (m, 1H), 2.50 – 2.48 (m, 4H);

^{13}C NMR (75 MHz, $CDCl_3$) δ 170.27, 164.99, 159.29, 156.61, 143.29, 142.65, 132.08, 127.43, 124.36, 121.14, 120.19, 111.01, 109.33, 57.30, 55.73, 54.43, 52.72, 50.23, 49.65, 46.00, 43.05. **HRMS** (ESI): *m/z* calculated for $C_{23}H_{24}N_4O_4SNa^+$ $[M + Na]^+$: 475.1410, found: 475.1411.

Preparation of (4-(1-(3-methoxy-4-(thiophen-3-yl)benzoyl)azetidin-3-yl)piperazin-1-yl)(thiazol-2-yl)methanone (22). Compound **22** was prepared in a manner similar to that described for **16** in 40% yield as a white solid. Melting point: 103 – 104 ºC. ^{1}H NMR (300 MHz, $CDCl_3$) δ 7.86 (d, *J* = 3.2 Hz, 1H), 7.67 (dd, *J* = 2.9, 1.2 Hz, 1H), 7.53 (d, *J* = 3.2 Hz, 1H), 7.49 (d, *J* = 7.9 Hz, 1H), 7.44 (dd, *J* = 5.0, 1.2 Hz, 1H), 7.38 – 7.31 (m, 2H), 7.17 (dd, *J* = 7.9, 1.5 Hz, 1H), 4.52 – 4.21 (m, 5H), 4.15 – 4.06 (m, 1H), 3.91 (s, 3H), 3.90 – 3.81 (m, 2H), 3.30 – 3.19 (m, 1H), 2.50 – 2.46 (m, 4H); ^{13}C NMR (75 MHz, $CDCl_3$) δ 170.26, 165.04, 159.32, 156.66, 143.30, 137.44, 132.77, 129.33, 128.41, 127.95, 124.89, 124.37, 120.18, 111.36, 57.36, 55.86, 54.43, 52.78, 50.25, 49.67, 46.08, 43.13. **HRMS** (ESI): *m/z* calculated for $C_{23}H_{24}N_4O_3S_2Na^+$ $[M + Na]^+$: 491.1182, found: 491.1180.

Preparation of (4-(1-(4-(3-fluoroazetidin-1-yl)benzoyl)azetidin-3-yl)piperazin-1-yl)(thiazol-2-yl)methanone (36). Compound **36** was prepared in a manner similar to that described for **16** in 32% yield as a white solid. Melting point: 171 – 172 ºC. ^{1}H NMR (300 MHz, $CDCl_3$) δ 7.85 (d, *J* = 2.8 Hz, 1H), 7.57 – 7.50 (m, 3H), 6.39 (d, *J* = 8.3 Hz, 2H), 5.64 – 5.23 (m, 1H), 4.56 – 3.93 (m, 10H), 3.82 (s, 2H), 3.27 – 3.13 (m, 1H), 2.48 – 2.43 (m, 4H); ^{19}F NMR (282 MHz, $CDCl_3$) δ -175.66 – -178.14 (m); ^{13}C NMR (75 MHz, $CDCl_3$) δ 170.69, 165.02, 159.27, 152.59, 143.25, 129.66, 124.28, 122.01, 110.78, 82.66 (d, *J* = 204.9 Hz), 59.30 (d, *J* = 24.2 Hz), 57.42, 54.41, 52.66, 50.18, 49.61, 46.07, 43.12. **HRMS** (ESI): *m/z* calculated for $C_{21}H_{24}FN_5O_2SNa^+$ $[M + Na]^+$: 452.1527, found: 452.1529.

Preparation of (4-(1-(4-(3-fluoropyrrolidin-1-yl)benzoyl)azetidin-3-yl)piperazin-1-yl)(thiazol-2-yl)methanone (37). Compound **37** was prepared in a manner similar to that described for

16 in 30% yield as a white solid. Melting point: 165 – 166 ºC. ^{1}H NMR (300 MHz, $CDCl_3$) δ 7.85 (d, *J* = 3.2 Hz, 1H), 7.63 – 7.48 (m, 3H), 6.50 (d, *J* = 8.8 Hz, 2H), 5.48 – 5.23 (m, 1H), 4.51 (s, 2H), 4.38 – 4.04 (m, 4H), 3.87 (s, 2H), 3.64 – 3.59 (m, 1H), 3.56 – 3.41 (m, 3H), 3.32 – 3.18 (m, 1H), 2.54 (s, 4H), 2.44 – 2.29 (m, 1H), 2.28 – 2.01 (m, 1H); ^{19}F NMR (282 MHz, $CDCl_3$) δ -170.11 – -171.72 (m); ^{13}C NMR (75 MHz, $CDCl_3$) δ 170.93, 165.07, 159.30, 149.29, 143.27, 129.99, 124.28, 120.18, 111.05, 92.86 (d, *J* = 176.1 Hz), 57.51, 54.49, 54.40 (d, *J* = 23.2 Hz), 52.59, 50.21, 49.64, 46.11, 45.36, 43.16, 32.38 (d, *J* = 21.8 Hz). **HRMS** (ESI): *m/z* calculated for $C_{22}H_{26}FN_5O_2SNa^+$ $[M + Na]^+$: 466.1683, found: 466.1685.

Preparation of (4-(1-(4-(4-fluoropiperidin-1-yl)benzoyl)azetidin-3-yl)piperazin-1-yl)(thiazol-2-yl)methanone (38). Compound **38** was prepared in a manner similar to that described for **16** in 19% yield as a white solid. Melting point: 137 – 138 ºC. ^{1}H NMR (300 MHz, $CDCl_3$) δ 7.86 (d, *J* = 3.2 Hz, 1H), 7.59 – 7.50 (m, 3H), 6.90 – 6.83 (m, 2H), 4.84 (ddt, *J* = 14.6, 9.8, 4.2 Hz, 1H), 4.54 – 4.04 (m, 6H), 3.84 (s, 2H), 3.52 – 3.14 (m, 5H), 2.47 (s, 4H), 2.10 – 1.83 (m, 4H); ^{19}F NMR (282 MHz, $CDCl_3$) δ -177.11 – -177.63 (m); ^{13}C NMR (75 MHz, $CDCl_3$) δ 170.49, 165.07, 159.30, 152.66, 143.28, 129.78, 124.30, 122.72, 114.49, 88.19 (d, *J* = 171.3 Hz), 57.40, 54.47, 52.65, 50.22, 49.65, 46.11, 88.19 (d, *J* = 171.3 Hz), 43.15, 30.82 (d, *J* = 19.8 Hz). **HRMS** (ESI): *m/z* calculated for $C_{23}H_{28}FN_5O_2SNa^+$ $[M + Na]^+$: 480.1840, found: 480.1841.

Pharmacology. The[^{3}H]2-OG hydrolysis assay was carried out using cytosolic preparation from rat brain according to our previous procedure.[41, 68] Briefly, the hydrolysis was measured as per the method described by Boldrup et al.,[69] whereby test compounds, brain samples and assay buffer (10 mM Tris-HCl and 1 mM EDTA, pH 7.4) are preincubated for 0-60 min prior to addition of substrate ([^{3}H]2-OG

for MAGL, obtained from American Radiolabeled Chemicals Inc. (St. Louis, MO, USA) and diluted with non-radioactive 2-OG, as appropriate (Cayman Chemical Co., Ann Arbor, MI, USA) to give the final assay concentration (0.5 μM in assay buffer containing 0.125% w/v assay concentration of fatty acid-free bovine serum albumin) in an assay volume of 200 μL. Reactions were stopped by addition of 400 μL of a solution containing active charcoal in 0.5 M HCl. Phases were separated by centrifugation and the aqueous phase, containing the reaction products, were taken and measured for tritium content using liquid scintillation spectroscopy with quench correction. pIC_{50} and hence IC_{50} values were determined on the data expressed as % of control using the log(inhibitor) vs. response - variable slope algorithm of GraphPad Prism. Using this assay, the prototypical MAGL inhibitor JZL184 inhibits rat cerebellar 2-OG hydrolysis with an IC_{50} value, following a 60 min preincubation phase, of 5.8 nM and a residual activity of ~10%).[68]

Statistical Analysis. Statistical analysis was performed by a student's two-tailed t-test, and we used asterisks to indicate statistical significance: $^{*}p < 0.05$, $^{**}p \leq 0.01$, $^{***}p \leq 0.001$, and $^{***}p \leq 0.0001$.

Activity-based Protein Profiling (ABPP). The general procedure for ABPP assays was described previously.[41, 70] Briefly, mouse brain membrane proteomes (1 mg/mL) were preincubated with either DMSO or inhibitors (1 μM and 10 μM) at 37 °C. After 30 min, FP-rhodamine (1 μM final concentration) was added, and the mixture was incubated for another 1−180 min at room temperature. Reactions were quenched with 4× SDS loading buffer and run on SDS−PAGE. Samples were visualized by in-gel fluorescence scanning using a ChemiDoc MP system. For time course experiment, proteomes are treated with 1 μM compounds **16−22**, **36-38** for 30 min at 37 °C followed by labeling with FP-Rh (1

μM final concentration) for varying time at room temperature. DMSO is negative control, and MJN110 [2,5-dioxopyrrolidin-1-yl 4-(bis(4-chlorophenyl)methyl) piperazine-1-carboxylate],[71] a validated irreversible MAGL inhibitor, is positive control. The relative intensity was compared to the DMSO treated proteomes, which were set to 100%. All data were acquired in average of 3 runs. The percentage of enzyme activity remaining was determined by measuring the integrated optical intensity of the fluorescent protein bands using image lab 5.2.1.

Binding Affinities to CB_1 and CB_2 Receptors. CB_1 and CB_2 binding profiles of **8**, **17** and **37** were determined according to published literatures[72, 73] and supported by the National Institute of Mental Health's Psychoactive Drug Screening Program. The detailed procedures "assay protocol book" are listed on the Web site (https://pdspdb.unc.edu/pdspWeb/). Compound CP55940 was used as positive control in CB1/CB2 agonist assays. Rimonabant was used as positive control in CB_1 antagonist assay, and SR144528 was used as positive control in CB_2 antagonist assay. All data were acquired in average of 3−5 runs. The results are shown in Table 1, and the corresponding dose-response curves are shown in Figure 4.

Molecular Docking Studies. Candidate compounds **8, 17 and 37** were docked onto the selected protein structure (PDB ID: 3PE6) using the Autodock Vina module in the UCSF Chimera software. Briefly, the mol2 file of protein was prepared by deleting the solvent, adding hydrogen atoms and charges using the default settings. Standard residues were determined according to the AMBER 14 force field, while non-standard residues were ignored. Note that the predicted free energy of binding was calculated in

AutoDock Vina using a hybrid scoring function (combined knowledge-based and empirical approaches).[74]

Measurement of Distribution Coefficient (LogD) ("shake flask method"). The general procedure for lipophilicity measurement was described previously[39, 41] with minor modification in this work. Briefly, the measurement of Log*D* values was carried out by mixing test compound (20 μM in DMSO, 50 μL) with *n*-octanol (475 μL) and PBS (475 μL) in a test tube. Both *n*-octanol and PBS were pre-saturated with each other prior to use. After vortexed for 1 min, the tube was shaken at 37 °C overnight. PBS phase and *n*-octanol phase were aliquoted (200 μL each). The amount of the test compound in each phase was determined by Agilent 6430 Triple Quad LC/MS. The Log*D* was calculated by Log [ratio between the amount of test compound in *n*-octanol and PBS].

Radiochemistry. Radiosynthesis of [^{11}C]8 (48) using [^{11}C]$COCl_2$ (1,1,1,3,3,3-hexafluoropropan-2-yl 3-(4-(thiazole-2-carbonyl)piperazin-1-yl)azetidine-1-carboxylate-^{11}C). The general procedure for [^{11}C]$COCl_2$ formation was described previously[39, 41] with minor modification in this work. Briefly, [^{11}C]CO_2 was produced by ^{14}N(p, α)^{11}C nuclear reactions in a cyclotron, and transferred into a pre-heated methanizer packed with nickel catalyst at 400 ºC to generate [^{11}C]CH_4, which was subsequently reacted with chlorine gas at 560 ºC to produce [^{11}C]CCl_4. [^{11}C]$COCl_2$ was generated by reacting [^{11}C]CCl_4 with iodine oxide and sulfuric acid,[39] and trapped in a solution of hexafluoroisopropanol (5.00 mg) and 1,2,2,6,6-pentamethylpiperidine (PMP; 5.4 μL) in THF (200 μL) at 0 °C. A solution of piperazinyl azetidine **7** (1.00 mg) and PMP (1.0 μL) in THF (200 μL) was added into the mixture and heated at 30 °C for 3 min before cooling to ambient temperature. The reaction mixtures were

concentrated to remove THF, then diluted with HPLC mobile phase (500 µL), followed by the injection into an HPLC column. HPLC purification was performed on a Capcell Pak C18 column (10 x 250 mm, 5 µm) using a mobile phase of CH_3CN / H_2O + 0.1% Et_3N (55/45, v/v) at a flowrate of 5.0 mL/min. The retention time of **48** was 8.5 min. The product solution was concentrated by evaporation and reformulated in a saline solution (3 mL) containing 100 µL of 25% ascorbic acid in sterile water and 100 µL of 20% Tween® 80 in ethanol. (Note: We added ascorbic acid to prevent potential radiolysis and Tween® 80 to improve aqueous solubility.) The radiochemical and chemical purity were measured by an analytical HPLC (Capcell Pak C18, 4.6 x 250 mm, 5µm). The identity of **48** was confirmed by the co-injection with unlabeled **8**. The radiochemical yield was 17.8 ± 10.7% (n = 6) decay-corrected based on starting [^{11}C]CO_2 with > 99% radiochemical purity and the molar activity was 29.7–52.4 GBq/µmol (0.83–1.41 Ci/µmol).

Radiosynthesis of [^{11}C]8 (48) using [^{11}C]CO_2 (1,1,1,3,3,3-hexafluoropropan-2-yl 3-(4-(thiazole-2-carbonyl)piperazin-1-yl)azetidine-1-carboxylate-^{11}C). The general experimental section was described previously[75] with minor modification as follows: ***(a) Set-up:*** Prior to the start-of-synthesis, a solution of dehydrating (0.2 µL, $POCl_3$) agent in MeCN (100 µL) were loaded into the reagent loop using a 1 mL syringe. Furthermore, to the same loop, additional amount of MeCN (800 µL) was added. A solution of the piperazinyl azetidine precursor **7**, BEMP (2.5 µL) in MeCN (40-50 µL), was loaded onto the reactor loop (section A). Furthermore, a solution of HFIP (50 µL) in MeCN (50 µL) was loaded onto another part of the reactor loop (section B). To enable reagent injection to the different sections of the reactor loop, the inlet nut on union-connectors were replaced by a needle injection port. It is important to note that prior to use, all solutions were de-gassed with helium flow for 15 min and kept over 4Å molecular sieves to minimize the introduction of atmospheric CO_2. ***(b)***

Trapping and reaction *(Synthetic procedure)*. [^{11}C]CO_2 was produced by ^{14}N(p, α)^{11}C nuclear reactions in a cyclotron, then transferred into a liquid nitrogen trap of [^{11}C]CO_2-fixation apparatus. The stainless-steel tube was removed from the liquid nitrogen by an air-pressure driven lift, whereby [^{11}C]CO_2 was passed through the coated reaction loop in a controlled stream of N_2 (20 mL/min). When radioactivity peaked in the reaction loop, as measured by the proximal radiation detector (typically within 2 min), the flow of N_2 was stopped and the reaction was allowed to proceed for an additional 1 min. Following the [^{11}C]carbamate ion formation, the position of the injection valve was switched and the content of the reagent loop was eluted into the reactor loop by a stream of nitrogen (80 mL/min), where the dehydration reagent ($POCl_3$) reacts with [^{11}C]carbamate ion to form an [^{11}C]isocyanate. Finally, the [^{11}C]anhydride reacts with the HFIP in section B of the reactor loop, to form the final ^{11}C-labelled product **48**. The crude reaction mixture is then eluted to an empty receiving vial pre-loaded with 3.5 mL of water and injected into a HPLC column. HPLC purification was performed on a ACE 5 C-18-HL column (10 x 250 mm, 5 μm, Waters) using a mobile phase of CH_3CN / 0.1 M $CH_3CO_2NH_4$ (55/45, v/v) at a flowrate of 5.0 mL/min. The retention time of **48** was 12 min. The radiochemical and chemical purity were measured by an analytical HPLC (XSelect HSS T3, 3.5 μm, 4.6 x 150mm, Waters). The identity of **48** was confirmed by the co-injection with unlabeled **8**. The radiochemical yield was 2.5 ± 0.4% (n = 2) decay-corrected based on starting [^{11}C]CO_2 with > 99% radiochemical purity and the molar activity was 288.6 ± 7.4 GBq/μmol (7.8±0.2 Ci/μmol).

Radiosynthesis of [^{11}C]17 (49) (^{11}C-carbonyl-labeled (4-(1-(4'-chloro-2-(methoxy-^{11}C)-3'-(trifluoromethyl)-[1,1'-biphenyl]-4-carbonyl)azetidin-3-yl)piperazin-1-yl)(thiazol-2-yl)methanone). The general procedure for [^{11}C]CH_3I formation was described previously[76] with minor modification in this work. Briefly, [^{11}C]CH_3I was synthesized from cyclotron-produced [^{11}C]CO_2, which was

produced by $^{14}N(p, \alpha)^{11}C$ nuclear reaction. $[^{11}C]CO_2$ was bubbled into a solution of $LiAlH_4$ (0.4 M in THF, 300 μL). After evaporation, the remaining reaction mixture was treated with hydroiodic acid (57% aqueous solution, 300 μL). The resulting $[^{11}C]CH_3I$ was transferred under helium gas with heating into a precooled (−15 to −20 °C) reaction vessel containing the phenolic precursor **47** (1.0 mg), NaOH (3.7 μL, 0.5 M), and anhydrous DMF (300 μL). After the radioactivity reached a plateau during transfer, the reaction vessel was warmed to 70 °C and maintained for 5 min. CH_3CN/H_2O + 0.1% Et_3N (v/v, 60/40, 0.5 mL) was added to the reaction mixture, which was then injected to a semipreparative HPLC system. HPLC purification was completed on a Capcell Pak UG80 C18 column (10 mm i.d. × 250 mm) using a mobile phase of CH_3CN/H_2O + 0.1% Et_3N (v/v,60/40) at a flow rate of 5.0 mL/min. The retention time for **49** was 9.8 min. The radioactive fraction corresponding to the desired product was collected in a sterile flask, evaporated to dryness in vacuo, and reformulated in a saline solution (3 mL) containing 100 μL of 25% ascorbic acid in sterile water and 100 μL of 20% Tween 80 in ethanol. (Note: We added ascorbic acid to prevent potential radiolysis and Tween 80 to improve aqueous solubility.) The synthesis time was ~30 min from the end of bombardment. Radiochemical and chemical purity were measured by analytical HPLC (Capcell Pak UG80 C18, 4.6 mm i.d. × 250 mm, UV at 254 nm; CH_3CN/H_2O + 0.1% Et_3N (v/v, 60/40) at a flow rate of 1.0 mL/min, retention time: 9.5 min). The identity of **49** was confirmed by the co-injection with unlabeled **17**. Radiochemical yield was 25 ± 8% (n = 3) decay-corrected based on $[^{11}C]CO_2$ with >99% radiochemical purity, and the molar activity was greater than 92.5 GBq/μmol (2.5 Ci/μmol).

Radiosynthesis of [^{18}F]37 (50) ((4-(1-(4-(3-(fluoro-^{18}F)pyrrolidin-1-yl)benzoyl)azetidin-3-yl)piperazin-1-yl)(thiazol-2-yl)methanone). The cyclotron-produced $[^{18}F]F^-$ was separated from $H_2{}^{18}O$ using the Sep-Pak Accell Plus QMA Plus Light cartridge (Waters; Milford, Ma). The produced

[^{18}F]F− was eluted from the cartridge with a mixture of aqueous K_2CO_3 (4 mg in 200 μL) and a solution of 4,7,13,16,21,24-hexaoxa-1,10-diazabicyclo[8,8,8]hexacosane (Kryptofix222; 7.5 mg) in CH_3CN (200 μL), and transferred to a reaction vessel in the hot cell. After drying [^{18}F]KF solution at 120 °C for 30 min to remove water and CH_3CN, a solution of mesylate precursor 50 (2.0 mg) in anhydrous DMSO(300 μL) was then added. The vessel was heated at 120 °C for 10 min, then diluted with HPCL mobile phase (500 μL), followed by the injection into an HPLC column. HPLC purification was performed on a X Bridge Prep C18 column (10 x 250 mm, 5 μm) using a mobile phase of CH_3CN / H_2O / Et_3N (30/70/0.1) at a flowrate of 5.0 mL/min. The reaction time of **50** was 13.5 min. The radioactive fraction corresponding to the desired product was collected in a sterile flask, evaporated to dryness in vacuo, and reformulated in a saline solution (3 mL) containing 100 μL of 25% ascorbic acid in sterile water and 100 μL of 20% Tween 80 in ethanol. (Note: We added ascorbic acid to prevent potential radiolysis and Tween 80 to improve aqueous solubility.) The synthesis time was 71 min from end of bombardment. Radiochemical and chemical purity were measured by analytical HPLC (X Bridge Prep C18 column (4.6 x 250 mm, 5 μm) using a mobile phase of CH_3CN / H_2O + 0.1% Et_3N (30/70) at a flow rate of 1.0 mL/min. The identity of **50** was confirmed by the co-injection with unlabeled **37**. Radiochemical yield was 39.3 ± 13.7% (n = 5) decay-corrected based on [^{18}F]F^- with >99% radiochemical purity, and the molar activity was 111.8 – 328.7 GBq/μmol (3.03–8.87 Ci/μmol).

Small-animal PET imaging studies. The general procedure for PET studies was described previously[39, 41] with minor modification in this work. Briefly, PET scans were carried out by an Inveon PET scanner (Siemens Medical Solutions, Knoxville, TN, USA). Sprague-Dawley rats were kept under anesthesia using 1-2% (v/v) isoflurane during the scan. The radiotracer (*ca.* 1 mCi / 150 μL) was injected into the

tail vein via a preinstalled catheter. A dynamic scan in 3D list mode was acquired for 90 min. For *pretreatment studies*, a solution of KML29 (3 mg/kg) in 300 μL saline containing 10% ethanol and 5% Tween® 80 was injected via the pre-embedded tail vein catheter at 30 min prior to tracer injection. As we previously reported, [39, 77, 78] the PET dynamic images were reconstructed using ASIPro VW software (Analysis Tools and System Setup/Diagnostics Tool, Siemens Medical Solutions). Volumes of interest, including the whole brain, hippocampus, cerebral cortex, cerebellum, striatum, thalamus, and pons were placed using ASIPro software. The radioactivity was decay-corrected and expressed as the standardized uptake value. SUV = (radioactivity per mL tissue / injected radioactivity) x body weight.

Ex vivo whole body biodistribution of 48-50 in mice. The general procedure for ex vivo biodistribution studies was described previously[39, 41] with minor modification in this work. Briefly, a solution of **48-50** (50 μCi / 150-200 μL) was injected into CD-1 mice via tail vein. These mice (each time point n = 4) were sacrificed at 5, 15, 30 and 60 min post tracer injection. Major organs, including whole brain, heart, liver, lung, spleen, kidneys, small intestine (including contents), muscle, testes, and blood samples were quickly harvested and weighted. The radioactivity present in these tissues was measured using 1480 Wizard gamma counter (PerkinElmer, USA), and all radioactivity measurements were automatically decay corrected based on the half-life of carbon-11. The results are expressed as the percentage of injected dose per gram of wet tissue (% ID/g).

Radiometabolite analysis. The general procedure for radiometabolite analysis was described previously[39, 41] with minor modification in this work. Briefly, Following the intravenous injection of tracers **48-50**, CD-1 mice were sacrificed at 30 min (*n* = 2). Either whole brain (for **48**) or blood (for **49** and **50**) samples were quickly removed and the blood samples were centrifuged at 15,000 x g for 2 min

at 4 °C to separate the plasma. The supernatant (0.5 mL) was then collected in a test tube containing CH_3CN (0.5 mL) and the resulting mixture was vortexed for 15s and centrifuged at 15,000 x g for 2 min for deproteinization. The rat brain was homogenized in an ice-cooled CH_3CN/H_2O (1 mL, 1/1, v/v) solution. The homogenate was centrifuged at 150,000 rpm for 2 min at 4 °C and the supernatant was collected. The recovery of radioactivity into the supernatant for all three tracers **48-50** was > 90% based on the total radioactivity in the brain or blood homogenate. An aliquot of the supernatant (100 μL) obtained from the plasma or brain homogenate was injected into the HPLC system together with unlabelled **8**, **17** or **37**, and analyzed using a Phenomenex C18 column (10.0 mm ID × 250 mm). The radioactivity collected was measured by a 1480 Wizard gamma counter (PerkinElmer, USA). The percentage of **48**, **49** or **50** to total radioactivity was calculated as (counts for **48**, **49** or **50**/total counts) × 100.

ASSOCIATED CONTENT

Supporting Information

The Supporting Information is available free of charge on the ACS Publications website at DOI:

Experimental procedures, characterization and NMR spectra of compounds **3**, **4**, **6**, **7**, **15b-g**, **24-35**, **40**, **42-47**, **51b-g** and **52**, and supplemental figures and tables (PDF)

Molecular formula strings and some data (CSV)

AUTHOR INFORMATION

Corresponding Author

* For S.H.L.: Tel: +1 617 726 6107. Fax: +1-617-726-6165. E-mail: liang.steven@mgh.harvard.edu.

* For M.-R.Z.: Tel: +81 433 823 709. Fax: +81-43-206-3261. E-mail: zhang.ming-rong@qst.go.jp.

Author Contributions

The manuscript was written through contributions of all the authors. All authors have given approval to the final version of the manuscript. [#]Z. Chen and W. Mori contributed equally.

Notes

The authors declare no competing financial interest.

ACKNOWLEDGMENTS

We thank Dr. Lei Zhang (Medicine Design, Pfizer, Inc) and Professor Thomas J. Brady (Nuclear Medicine and Molecular Imaging, Radiology, MGH and Harvard Medical School) for helpful discussion. We also thank the National Institute of Mental Health's Psychoactive Drug Screening Program (NIMH PDSP; directed by Bryan L. Roth at the University of North Carolina at Chapel Hill and Jamie Driscoll at NIMH) for *in vitro* screening. We thank Mona Svensson for expert technical assistance in the [^{3}H]2-OG hydrolysis studies. Financial support from the NIH grants (DA038000 and DA043507 to S.L., AG054473 to N.V., and DA033760 to B.F.C.), CSC scholarship to Z. C. (Grant No. 201606250107) and the Swedish Science Research Council (Grant 12158, Medicine) is gratefully acknowledged.

ABBREVIATIONS

MAGL, monoacylglycerol lipase; eCB, endocannabinoid system; CNS, central nervous system; 2-AG, 2-arachidonylglycerol; AEA, anandamide; FAAH, fatty acid amide hydrolase; 2-OG, 2-oloeylglyverol; PET, positron emission tomography; SUV, standardized uptake value; TAC, time-activity curve; %ID/g,

the percentage of injected dose per gram of wet tissue; PgP, P-glycoprotein; Bcrp, breast cancer resistance protein.

REFERENCES

1. Matsuda, L. A.; Lolait, S. J.; Brownstein, M. J.; Young, A. C.; Bonner, T. I. Structure of a cannabinoid receptor and function expression of the cloned cDNA. *Nature* **1990,** 346, 561-564.

2. Cravatt, B. F.; Lichtman, A. H. The endogenous cannabinoid system and its role in nociceptive behavior. *J. Neurobio.* **2004,** 61, 149-160.

3. Pertwee, R. The pharmacology of cannabinoid receptors and their ligands: an overview. *Int. J. Obesity* **2006,** 30, S13-S18.

4. Ahn, K.; McKinney, M. K.; Cravatt, B. F. Enzymatic pathways that regulate endocannabinoid signaling in the nervous system. *Chem. Rev.* **2008,** 108, 1687-1707.

5. Aaltonen, N.; Ribas, C. R.; Lehtonen, M.; Savinainen, J. R.; Laitinen, J. T. Brain regional cannabinoid CB_1 receptor signalling and alternative enzymatic pathways for 2-arachidonoylglycerol generation in brain sections of diacylglycerol lipase deficient mice. *Eur. J. Pharm. Sci.* **2014,** 51, 87-95.

6. Hohmann, A. G.; Suplita, R. L. Endocannabinoid mechanisms of pain modulation. *AAPS. J.* **2006,** 8, E693-E708.

7. Bisogno, T.; Di Marzo, V. Short- and long-term plasticity of the endocannabinoid system in neuropsychiatric and neurological disorders. *Pharmacol. Res.* **2007,** 56, 428-442.

8. Di Marzo, V.; Petrosino, S. Endocannabinoids and the regulation of their levels in health and disease. *Curr. Opin. Lipidol.* **2007,** 18, 129-140.

9. Jhaveri, M. D.; Richardson, D.; Chapman, V. Endocannabinoid metabolism and uptake: novel targets for neuropathic and inflammatory pain. *Br. J. Pharmacol.* **2007,** 152, 624-632.

10. Lambert, D. M. Allergic contact dermatitis and the endocannabinoid system: from mechanisms to skin care. *ChemMedChem* **2007,** 2, 1701-1702.

11. Moreira, F. A.; Grieb, M.; Lutz, B. Central side-effects of therapies based on CB_1 cannabinoid receptor agonists and antagonists: focus on anxiety and depression. *Best Pract. Res. Clin. Endocrinol. Metab.* **2009,** 23, 133-144.

12. Owens, B. Drug development: The treasure chest. *Nature* **2015,** 525, S6-S8.

13. Cravatt, B. F.; Giang, D. K.; Mayfield, S. P.; Boger, D. L.; Lerner, R. A.; Gilula, N. B. Molecular characterization of an enzyme that degrades neuromodulatory fatty-acid amides. *Nature* **1996,** 384, 83-87.

14. McKinney, M. K.; Cravatt, B. F. Structure and function of fatty acid amide hydrolase. *Annu. Rev. Biochem.* **2005,** 74, 411-432.

15. Blankman, J. L.; Simon, G. M.; Cravatt, B. F. A comprehensive profile of brain enzymes that hydrolyze the endocannabinoid 2-arachidonoylglycerol. *Chem. Biol.* **2007,** 14, 1347-1356.

16. Kohnz, R. A.; Nomura, D. K. Chemical approaches to therapeutically target the metabolism and signaling of the endocannabinoid 2-AG and eicosanoids. *Chem. Soc. Rev.* **2009,** 43, 6859-6869.

17. Labar, G.; Wouters, J.; Lambert, D. M. A review on the monoacylglycerol lipase: at the interface between fat and endocannabinoid signaling. *Curr. Med. Chem.* **2010,** 17, 2588-2607.

18. Karlsson, M.; Contreras, J. A.; Hellman, U.; Tornqvist, H.; Holm, C. cDNA cloning, tissue distribution, and identification of the catalytic triad of monoglyceride lipase: evolutionary relationship to esterases, lysophospholipases, and haloperoxidases. *J. Biol. Chem.* **1997,** 272, 27218-27223.

19. Dinh, T. P.; Carpenter, D.; Leslie, F. M.; Freund, T. F.; Katona, I.; Sensi, S. L.; Kathuria, S.; Piomelli, D. Brain monoglyceride lipase participating in endocannabinoid inactivation. *Proc. Natl. Acad. Sci.* **2002,** 99, 10819-10824.

20. Long, J. Z.; Li, W.; Booker, L.; Burston, J. J.; Kinsey, S. G.; Schlosburg, J. E.; Pavón, F. J.; Serrano, A. M.; Selley, D. E.; Parsons, L. H.; Lichtman, A. H.; Cravatt, B. F. Selective blockade of 2-arachidonoylglycerol hydrolysis produces cannabinoid behavioral effects. *Nat. Chem. Biol.* **2009,** 5, 37-44.

21. Long, J. Z.; Nomura, D. K.; Cravatt, B. F. Characterization of monoacylglycerol lipase inhibition reveals differences in central and peripheral endocannabinoid metabolism. *Chem. Biol.* **2009,** 16, 744-753.

22. Nomura, D. K.; Long, J. Z.; Niessen, S.; Hoover, H. S.; Ng, S.-W.; Cravatt, B. F. Monoacylglycerol lipase regulates a fatty acid network that promotes cancer pathogenesis. *Cell* **2010,** 140, 49-61.

23. Nomura, D. K.; Lombardi, D. P.; Chang, J. W.; Niessen, S.; Ward, A. M.; Long, J. Z.; Hoover, H. H.; Cravatt, B. F. Monoacylglycerol lipase exerts dual control over endocannabinoid and fatty acid pathways to support prostate cancer. *Chem. Biol.* **2011,** 18, 846-856.

24. Nomura, D. K.; Morrison, B. E.; Blankman, J. L.; Long, J. Z.; Kinsey, S. G.; Marcondes, M. C.; Ward, A. M.; Hahn, Y. K.; Lichtman, A. H.; Conti, B.; Cravatt, B. F. Endocannabinoid hydrolysis generates brain prostaglandins that promote neuroinflammation. *Science* **2011,** 334, 809-813.

25. Ye, L.; Zhang, B.; Seviour, E. G.; Tao, K.-x.; Liu, X.-h.; Ling, Y.; Chen, J.-y.; Wang, G.-b. Monoacylglycerol lipase (MAGL) knockdown inhibits tumor cells growth in colorectal cancer. *Cancer Lett.* **2011,** 307, 6-17.

26. Chen, R.; Zhang, J.; Wu, Y.; Wang, D.; Feng, G.; Tang, Y. P. Monoacylglycerol lipase is a therapeutic target for Alzheimer's disease. *Cell Rep.* **2012,** 2, 1329-1339.

27. Jung, K.-M.; Clapper, J. R.; Fu, J.; D'Agostino, G.; Guijarro, A.; Thongkham, D.; Avanesian, A.; Astarita, G.; DiPatrizio, N. V.; Frontini, A.; Cinti, S.; Diano, S.; Piomelli, D. 2-Arachidonoylglycerol signaling in forebrain regulates systemic energy metabolism. *Cell Metab.* **2012,** 15, 299-310.

28. Cao, Z.; Mulvihill, M. M.; Mukhopadhyay, P.; Xu, H.; Erdélyi, K.; Hao, E.; Holovac, E.; Haskó, G.; Cravatt, B. F.; Nomura, D. K.; Pacher, P. Monoacylglycerol lipase controls endocannabinoid and eicosanoid signaling and hepatic injury in mice. *Gastroenterology* **2013,** 144, 808-817.

29. Costola-de-Souza, C.; Ribeiro, A.; Ferraz-de-Paula, V.; Calefi, A. S.; Aloia, T. P. A.; Gimenes-Júnior, J. A.; Almeida, V. I. d.; Pinheiro, M. L.; Palermo-Neto, J. Monoacylglycerol lipase (MAGL) inhibition attenuates acute lung injury in mice. *PLoS One* **2013,** 8, e77706.

30. Griebel, G.; Pichat, P.; Beeske, S.; Leroy, T.; Redon, N.; Jacquet, A.; Francon, D.; Bert, L.; Even, L.; Lopez-Grancha, M.; Tolstykh, T.; Sun, F.; Yu, Q.; Brittain, S.; Arlt, H.; He, T.; Zhang, B.; Wiederschain, D.; Bertrand, T.; Houtmann, J.; Rak, A.; Vallee, F.; Michot, N.; Auge, F.; Menet, V.; Bergis, O. E.; George, P.; Avenet, P.; Mikol, V.; Didier, M.; Escoubet, J. Selective blockade of the hydrolysis of the endocannabinoid 2-arachidonoylglycerol impairs learning and memory performance while producing antinociceptive activity in rodents. *Sci. Rep.* **2015,** 5, 7642.

31. Mulvihill, M. M.; Nomura, D. K. Therapeutic potential of monoacylglycerol lipase inhibitors. *Life Sci.* **2013,** 92, 492-497.

32. Ametamey, S. M.; Honer, M.; Schubiger, P. A. Molecular imaging with PET. *Chem. Rev.* **2008,** 108, 1501-1516.

33. Willmann, J. K.; van Bruggen, N.; Dinkelborg, L. M.; Gambhir, S. S. Molecular imaging in drug development. *Nat. Rev. Drug Discov.* **2008,** 7, 591-607.

34. Miller, P. W.; Long, N. J.; Vilar, R.; Gee, A. D. Synthesis of ^{11}C, ^{18}F, ^{15}O, and ^{13}N radiolabels for positron emission tomography. *Angew. Chem., Int. Ed.* **2008,** 47, 8998-9033.

35. Hicks, J. W.; Parkes, J.; Tong, J.; Houle, S.; Vasdev, N.; Wilson, A. A. Radiosynthesis and ex vivo evaluation of [^{11}C-carbonyl]carbamate- and urea-based monoacylglycerol lipase inhibitors. *Nucl. Med. Biol.* **2014,** 41, 688-694.

36. Test Re-Test Reliability of [^{11}C]PF-06809247 as a Novel PET Tacer. https://clinicaltrials.gov/ct2/show/NCT03100136?term=MAGL&rank=1 (accessed Apr 4, 2017).

37. Wang, L.; Mori, W.; Cheng, R.; Yui, J.; Rotstein, B. H.; Fujinaga, M.; Hatori, A.; Vasdev, N.; Zhang, M.-R.; Liang, S. H. A novel class of sulfonamido [^{11}C-carbonyl]-labeled carbamates and ureas as radiotracers for monoacylglycerol lipase. *J. Nucl. Med.* **2016,** 57, 4.

38. Wang, C.; Placzek, M. S.; Van de Bittner, G. C.; Schroeder, F. A.; Hooker, J. M. A novel radiotracer for imaging monoacylglycerol lipase in the brain using positron emission tomography. *ACS Chem. Neurosci.* **2016,** 7, c484-489.

39. Wang, L.; Mori, W.; Cheng, R.; Yui, J.; Hatori, A.; Ma, L.; Zhang, Y.; Rotstein, B. H.; Fujinaga, M.; Shimoda, Y.; Yamasaki, T.; Xie, L.; Nagai, Y.; Minamimoto, T.; Higuchi, M.; Vasdev, N.; Zhang, M.-R.; Liang, S. H. Synthesis and preclinical evaluation of sulfonamido-based [^{11}C-carbonyl]-carbamates and ureas for imaging monoacylglycerol lipase. *Theranostics* **2016,** 6, 1145-1159.

40. Ahamed, M.; Attili, B.; Veghel, D. V.; Ooms, M.; Berben, P.; Celen, S.; Koole, M.; Declercq, L.; Savinainen, J. R.; Laitinen, J. T.; Verbruggen, A.; Bormans, G. Synthesis and preclinical evaluation of

[^{11}C]MA-PB-1 for in vivo imaging of brain monoacylglycerol lipase (MAGL). *Eur. J. Med. Chem.* **2017,** 136, 104-113.

41. Cheng, R.; Mori, W.; Ma, L.; Alhouayek, M.; Hatori, A.; Zhang, Y.; Ogasawara, D.; Yuan, G.; Chen, Z.; Zhang, X.; Shi, H.; Yamasaki, T.; Xie, L.; Kumata, K.; Fujinaga, M.; Nagai, Y.; Minamimoto, T.; Svensson, M.; Wang, L.; Du, Y.; Ondrechen, M. J.; Vasdev, N.; Cravatt, B. F.; Fowler, C.; Zhang, M.-R.; Liang, S. H. In vitro and in vivo evaluation of ^{11}C-labeled azetidinecarboxylates for imaging monoacylglycerol lipase by PET imaging studies. *J. Med. Chem.* **2018,** 61, 2278-2291.

42. Wager, T. T.; Chandrasekaran, R. Y.; Hou, X.; Troutman, M. D.; Verhoest, P. R.; Villalobos, A.; Will, Y. Defining desirable central nervous system drug space through the alignment of molecular properties, in vitro ADME, and safety attributes. *ACS Chem. Neurosci.* **2010,** 1, 420-434.

43. Labar, G.; Wouters, J.; Lambert., D. M. A review on the monoacylglycerol lipase: at the interface between fat and endocannabinoid signalling. *Curr. Med. Chem.* **2010,** 17, 2588-2607.

44. Innis, R. B.; Cunningham, V. J.; Delforge, J.; Fujita, M.; Gjedde, A.; Gunn, R. N.; Holden, J.; Houle, S.; Huang, S.-C.; Ichise, M.; Iida, H.; Ito, H.; Kimura, Y.; Koeppe, R. A.; Knudsen, G. M.; Knuuti, J.; Lammertsma, A. A.; Laruelle, M.; Logan, J.; Maguire, R. P.; Mintun, M. A.; Morris, E. D.; Parsey, R.; Price, J. C.; Slifstein, M.; Sossi, V.; Suhara, T.; Votaw, J. R.; Wong, D. F.; Carson, R. E. Consensus nomenclature for in vivo imaging of reversibly binding radioligands. *J. Cereb. Blood Flow Metab.* **2007,** 27, 1533-1539.

45. Pike, V. W. PET radiotracers: crossing the blood-brain barrier and surviving metabolism. *Trends Pharmacol. Sci.* **2009,** 30, 431-440.

46. Schneider, G.; Neidhart, W.; Giller, T.; Schmid, G. "Scaffold hopping" by topological pharmacophore search: a contribution to virtual screening. *Angew. Chem. Int. Ed.* **1999,** 38, 2894-2896.

47. Hu, Y.; Stumpfe, D.; Bajorath, J. Recent advances in scaffold hopping. *J. Med. Chem.* **2017,** 60, 1238-1246.

48. Chevalier, K. M.; Dax, S. L.; Flores, C. M.; Liu, L.; Macielag, M. J.; McDonnell, M. E.; Nelen, M. I.; Prouty, S.; Todd, M.; Zhang, S.-P.; Zhu, B.; Nulton, E. L.; J. Clemente. Preparation of (Hetero)aromatic Piperazinyl Azetidinyl Amides as Monoacylglycerol Lipase (MGL) Inhibitors. WO2010124121, 2010.

49. Flores, C. M.; Nelen, M. I.; Nulton, E. L.; Prouty, S.; Todd, M.; Zhang, S.-P. Heteroaromatic and Aromatic Piperazinyl Azetidinyl Amides as Monoacylglycerol Lipase Inhibitors. WO2010124122, 2010.

50. Wang, L.; Fujinaga, M.; Cheng, R.; Yui, J.; Shimoda, Y.; Rotstein, B.; Zhang, Y.; Vasdev, N.; Zhang, M.-R.; Liang, S. Synthesis and preliminary evaluation of a ^{11}C-labeled piperidin-4-yl azetidine diamide for imaging monoacylglycerol lipase. *J. Nucl. Med.* **2016,** 57, 1044.

51. Cravatt, B. F.; Wright, A. T.; Kozarich, J. W. Activity-based protein profiling: from enzyme chemistry to proteomic chemistry. *Annu. Rev. Biochem.* **2008,** 77, 383-414.

52. Copeland, R. A.; Basavapathruni, A.; Moyer, M.; Scott, M. P. Impact of enzyme concentration and residence time on apparent activity recovery in jump dilution analysis. *Anal. Biochem.* **2011,** 416, 206-210.

53. Waterhouse, R. N. Determination of lipophilicity and its use as a predictor of blood-brain barrier penetration of molecular imaging agents. *Mol. Imaging Biol.* **2003,** 5, 376-389.

54. Patel, S.; Gibson, R. In vivo site-directed radiotracers: a mini-review. *Nucl. Med. Biol.* **2008,** 35, 805-815.

55. Pike, V. W. Considerations in the development of reversibly binding PET radioligands for brain imaging. *Curr. Med. Chem.* **2016,** 23, 1818-1869.

56. *Test No. 107: Partition Coefficient (n-octanol/water): Shake Flask Method*. Organisation for Economic Cooperation and Development (OECD): Paris, 1995.

57. Schalk-Hihi, C.; Schubert, C.; Alexander, R.; Bayoumy, S.; Clemente, J. C.; Deckman, I.; DesJarlais, R. L.; Dzordzorme, K. C.; Flores, C. M.; Grasberger, B.; Kranz, J. K.; Lewandowski, F.; Liu, L.; Ma, H.; Maguire, D.; Macielag, M. J.; McDonnell, M. E.; Mezzasalma Haarlander, T.; Miller, R.; Milligan, C.; Reynolds, C.; Kuo, L. C. Crystal structure of a soluble form of human monoglyceride lipase in complex with an inhibitor at 1.35 Å resolution. *Protein Sci.* **2011,** 20, 670-683.

58. Wilson, A. A.; Garcia, A.; Parkes, J.; Houle, S.; Tong, J.; Vasdev, N. [^{11}C]CURB: Evaluation of a novel radiotracer for imaging fatty acid amide hydrolase by positron emission tomography. *Nucl. Med. Biol.* **2011,** 38, 247-253.

59. Wilson, A. A.; Hicks, J. W.; Sadovski, O.; Parkes, J.; Tong, J.; Houle, S.; Fowler, C. J.; Vasdev, N. Radiosynthesis and evaluation of [^{11}C-carbonyl]-labeled carbamates as fatty acid amide hydrolase radiotracers for positron emission tomography. *J. Med. Chem.* **2013,** 56, 201-209.

60. Dahl, K.; Collier, T. L.; Cheng, R.; Zhang, X.; Sadovski, O.; Liang, S. H.; Vasdev, N. "In-loop" [^{11}C]CO_2 fixation: Prototype and proof of concept. *J. Label. Comp. Radiopharm.* **2018,** 61, 252-262.

61. Fowler, J. S.; MacGregor, R. R.; Wolf, A. P.; Arnett, C. D.; Dewey, S. L.; Schlyer, D.; Christman, D.; Logan, J.; Smith, M.; Sachs, H.; Aquilonius, S. M.; Bjurling, P.; Halldin, C.; Hartvig, P.; Leenders, K. L.; Lundqvist, H.; Oreland, L.; Stålnacke, C.-G.; Långström, B. Mapping human brain monoamine oxidase A and B with ^{11}C-labeled suicide inactivators and PET. *Science* **1987,** 235, 481-485.

62. Karlsson, M.; Contreras, J. A.; Hellman, U.; Tornqvist, H.; Holm, C. cDNA cloning, tissue distribution, and identification of the catalytic triad of monoglyceride lipase. Evolutionary relationship to esterases, lysophospholipases, and haloperoxidases. *J. Biol. Chem.* **1997,** 272, 27218-27223.

63. Wager, T. T.; Hou, X.; Verhoest, P. R.; Villalobos, A. Moving beyond rules: the development of a central nervous system multiparameter optimization (CNS MPO) approach to enable alignment of druglike properties. *ACS Chem. Neurosci.* **2010,** 1, 435-449.

64. Zhang, L.; Villalobos, A.; Beck, E. M.; Bocan, T.; Chappie, T. A.; Chen, L.; Grimwood, S.; Heck, S. D.; Helal, C. J.; Hou, X.; Humphrey, J. M.; Lu, J.; Skaddan, M. B.; McCarthy, T. J.; Verhoest, P. R.; Wager, T. T.; Zasadny, K. Design and selection parameters to accelerate the discovery of novel central nervous system positron emission tomography (PET) ligands and their application in the development of a novel phosphodiesterase 2A PET ligand. *J. Med. Chem.* **2013,** 56, 4568-4579.

65. Wager, T. T.; Hou, X.; Verhoest, P. R.; Villalobos, A. Central nervous system multiparameter optimization desirability: application in drug discovery. *ACS Chem. Neurosci.* **2016,** 7, 767-775.

66. McAllister, L. A.; Butler, C. R.; Mente, S.; O'Neil, S. V.; Fonseca, K. R.; Piro, J. R.; Cianfrogna, J. A.; Foley, T. L.; Gilbert, A. M.; Harris, A. R.; Helal, C. J.; Johnson, D. S.; Montgomery, J. I.; Nason, D. M.; Noell, S.; Pandit, J.; Rogers, B. N.; Samad, T. A.; Shaffer, C. L.; da Silva, R. G.; Uccello, D. P.; Webb, D.; Brodney, M. A. Discovery of trifluoromethyl glycol carbamates as potent and selective covalent monoacylglycerol lipase (MAGL) inhibitors for treatment of neuroinflammation. *J. Med. Chem.* **2018,** 61, 3008-3026.

67. Baell, J. B.; Holloway, G. A. New substructure filters for removal of pan assay interference compounds (PAINS) from screening libraries and for their exclusion in bioassays. *J. Med. Chem.* **2010,** 53, 2719-2740.

68. Bjorklund, E.; Noren, E.; Nilsson, J.; Fowler, C. J. Inhibition of monoacylglycerol lipase by troglitazone, *N*-arachidonoyl dopamine and the irreversible inhibitor JZL184: comparison of two different assays. *Br. J. Pharmacol.* **2010,** 161, 1512-1526.

69. Boldrup, L.; Wilson, S. J.; Barbier, A. J.; Fowler, C. J. A simple stopped assay for fatty acid amide hydrolase avoiding the use of a chloroform extraction phase. *J. Biochem. Biophys. Methods* **2004,** 60, 171-177.

70. Cravatt, B. F.; Wright, A. T.; Kozarich, J. W. Activity-based protein profiling: from enzyme chemistry to proteomic chemistry. *Annu. Rev. Biochem.* **2008,** 77, 383-414.

71. Niphakis, M. J.; Cognetta, A. B.; Chang, J. W.; Buczynski, M. W.; Parsons, L. H.; Byrne, F.; Burston, J. J.; Chapman, V.; Cravatt, B. F. Evaluation of NHS carbamates as a potent and selective class of endocannabinoid hydrolase inhibitors. *ACS Chem.Neurosci.* **2013,** 4, 1322-1332.

72. Besnard, J.; Ruda, G. F.; Setola, V.; Abecassis, K.; Rodriguiz, R. M.; Huang, X.-P.; Norval, S.; Sassano, M. F.; Shin, A. I.; Webster, L. A.; Simeons, F. R. C.; Stojanovski, L.; Prat, A.; Seidah, N. G.; Constam, D. B.; Bickerton, G. R.; Read, K. D.; Wetsel, W. C.; Gilbert, I. H.; Roth, B. L.; Hopkins, A. L. Automated design of ligands to polypharmacological profiles. *Nature* **2012,** 492, 215-220.

73. Kroeze, W. K.; Sassano, M. F.; Huang, X.-P.; Lansu, K.; McCorvy, J. D.; Giguère, P. M.; Sciaky, N.; Roth, B. L. PRESTO-Tango as an open-source resource for interrogation of the druggable human GPCRome. *Nat. Struct. Mol. Biol.* **2015,** 22, 362-369.

74. Trott, O.; Olson, A. J. AutoDock Vina: Improving the speed and accuracy of docking with a new scoring function, efficient optimization, and multithreading. *J. Comput. Chem.* **2009,** 31, 455-461.

75. Dahl, K.; Collier, T. L.; Cheng, R.; Zhang, X.; Sadovski, O.; Liang, S. H.; Vasdev, N. "In-loop" [^{11}C]CO_2 fixation: Prototype and proof of concept. *J. Label. Compd. Radiopharm.* **2017,** 61, 252-262.

76. Zhang, X.; Kumata, K.; Yamasaki, T.; Cheng, R.; Hatori, A.; Ma, L.; Zhang, Y.; Xie, L.; Wang, L.; Kang, H. J.; Sheffler, D. J.; Cosford, N. D. P.; Zhang, M.-R.; Liang, S. H. Synthesis and preliminary studies of a novel negative allosteric modulator, 7-((2,5-dioxopyrrolidin-1-yl)methyl)-4-(2-fluoro-4-[^{11}C]methoxyphenyl) quinoline-2-carboxamide, for imaging of metabotropic glutamate receptor 2. *ACS Chem. Neurosci.* **2017,** 8, 1937-1948.

77. Wang, L.; Yui, J.; Wang, Q.; Zhang, Y.; Mori, W.; Shimoda, Y.; Fujinaga, M.; Kumata, K.; Yamasaki, T.; Hatori, A.; Rotstein, B. H.; Collier, T. L.; Ran, C.; Vasdev, N.; Zhang, M.-R.; Liang, S. H. Synthesis and preliminary PET imaging studies of a FAAH radiotracer ([^{11}C]MPPO) based on α-ketoheterocyclic scaffold. *ACS Chem. Neurosci.* **2016,** 7, 109-118.

78. Chen, Z.; Mori, W.; Zhang, X.; Yamasaki, T.; Dunn, P. J.; Zhang, G.; Fu, H.; Shao, T.; Zhang, Y.; Hatori, A.; Ma, L.; Fujinaga, M.; Xie, L.; Deng, X.; Li, H.; Yu, Q.; Rong, J.; Josephson, L.; Ma, J.-A.; Shao, Y.; Tomita, S.; Zhang, M.-R.; Liang, S. H. Synthesis, pharmacology and preclinical evaluation of ^{11}C-labeled 1,3-dihydro-2*H*-benzo[d]imidazole-2-ones for imaging γ8-dependent transmembrane AMPA receptor regulatory protein. *Eur. J. Med. Chem.* **2018,** 157, 898-908.

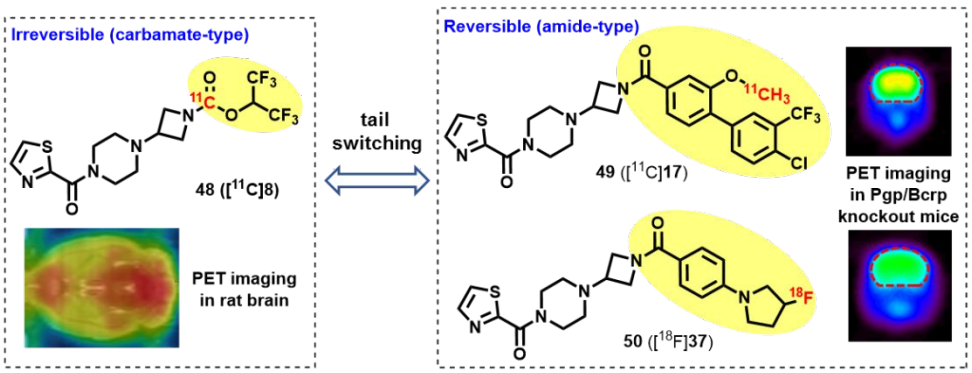

Table of Content graphic